Chemical Geology 593 (2022) 120754

Contents lists available at ScienceDirect

Chemical Geology

journal homepage: www.elsevier.com/locate/chemgeo

U-Pb isotopic dating of cassiterite: Development of reference materials and in situ applications by LA-SF-ICP-MS

Ming Yang [a,b,c], Rolf L. Romer [d,*], Yue-Heng Yang [a,b,c,**], Shi-Tou Wu [a,b], Hao Wang [a,b,c], Jia-Run Tu [e], Hong-Ying Zhou [e], Lie-Wen Xie [a,b], Chao Huang [a,b], Lei Xu [a,b], Jin-Hui Yang [a,b,c], Fu-Yuan Wu [a,b,c]

[a] State Key Laboratory of Lithospheric Evolution, Institute of Geology and Geophysics, Chinese Academy of Sciences, P. B. 9825, Beijing 100029, PR China
[b] Institutions of Earth Sciences, Chinese Academy of Sciences, Beijing 100029, PR China
[c] College of Earth and Planetary Sciences, University of Chinese Academy of Sciences, Beijing 100049, China
[d] GFZ German Research Centre for Geosciences, Telegrafenberg, Potsdam 14473, Germany
[e] Tianjin Center, China Geological Survey, Tianjin 300170, China

ARTICLE INFO

Keywords:
Cassiterite
U-Pb dating
^{208}Pb correction
LA-SF-ICP-MS
Reference materials

ABSTRACT

Cassiterite, the economically most important tin mineral, typically has moderate U and variable common Pb contents, making it amenable for U—Pb dating. Cassiterite has extremely low Th/U ratios (Th/U < 0.01) and its ^{208}Pb is dominantly common Pb. This is particularly helpful as there is significant interference of tungsten oxides on ^{202}Hg and ^{204}Pb. The feasibility of the ^{208}Pb correction procedure is discussed in detail. The ^{208}Pb corrected LA-SF-ICP-MS data are in good agreement with intercept ages in the Tera-Wasserburg diagram and ^{207}Pb corrected ages.

Twelve cassiterite samples were investigated using the ID-TIMS and LA-SF-ICP-MS methods. The ID-TIMS results of Pit-AB, Rond-A, RG-114, BB#7 and 19GX cassiterite are reported for the first time in this study. RG-114, BB#7 and 19GX cassiterite have very low common Pb contents and are recommended for use as primary reference materials for in situ cassiterite. Pit-AB, Rond-A and Yankee cassiterite contain a small amount of common Pb, produce reliable and consistent ages and are suitable as primary reference materials. The remaining five cassiterite samples (Kard, Zinnwald, Els, XBD-W and Y724) were only investigated using the LA-SF-ICP-MS method and produce ages consistent with published age data from the host rocks associated with the tin deposits and with published U—Pb ages of cassiterite from the same deposits. We present an ID-TIMS U—Pb of 154.3 ± 0.7 Ma for the commonly used cassiterite reference material AY-4. This age differs from previously reported ID-TIMS ages. This age discrepancy is caused by different initial common Pb compositions rather than age heterogeneity.

1. Introduction

Tin is a critical resource as it is widely used in electronics, chemical, and aerospace industries and many important high-tech fields. Tin is mostly extracted from cassiterite (SnO_2) which occurs in hydrothermal veins, pegmatites associated with granite intrusions, greisen, skarn and placer deposits (Lehmann, 1982; Jiang et al., 2020). A better understanding of the geological conditions of the formation of Sn deposits is essential for tin exploration. Dating cassiterite mineralization provides an indispensable step in connecting the formation of Sn resources to the magmatic and tectonic history of an area. Cassiterite often contains moderate amount of U and tends to exclude initial Pb (Swart and Moore, 1982; Zagruzina et al., 1987) and has robust U—Pb isotope systematics as it is resistant to alteration and has a high closure temperature comparable to zircon (Zhang et al., 2011; Neymark et al., 2021), which allows for direct U—Pb dating of Sn deposits.

Cassiterite U—Pb dating by isotope dilution thermal ionization mass spectrometry (ID-TIMS) was first carried out by Gulson and Jones

* Corresponding author.
** Corresponding author at: State Key Laboratory of Lithospheric Evolution, Institute of Geology and Geophysics, Chinese Academy of Sciences, P. B. 9825, Beijing 100029, PR China.
E-mail addresses: romer@gfz-potsdam.de (R.L. Romer), yangyueheng@mail.iggcas.ac.cn (Y.-H. Yang).

https://doi.org/10.1016/j.chemgeo.2022.120754
Received 3 October 2021; Received in revised form 28 January 2022; Accepted 30 January 2022
Available online 3 February 2022

(1992). These authors presented ages of ~2.1 Ga and ~ 250 Ma cassiterite from the Bushveld Complex in South Africa and from the Southeast Asia Tin Belt (Belitung Island in Indonesia), respectively. Liu et al. (2007a, 2007b) and Yuan et al. (2008, 2011) and Deng et al. (2017) adapted the method of Gulson and Jones (1992) to establish a procedure for cassiterite U—Pb dating by ID-TIMS. Cassiterite is very resistant to acid dissolution. Therefore, the use of concentrated HCl in autoclaves at 200 °C commonly does not decompose cassiterite completely (Gulson and Jones, 1992; Yuan et al., 2008, 2011; Rizvanova et al., 2017). Higher temperatures favour decomposition of cassiterite using concentrated HCl and autoclaves, however, the temperature is limited by the thermal stability of the Teflon beakers (240 °C). Rizvanova and Kuznetsov (2020) managed to completely decompose the cassiterite at 240 °C in 24 h. Hydroiodic acid (HI) is effective to decompose cassiterite at a relatively low temperature of 100 °C (Caley, 1932). Yamazaki et al. (2013) claimed complete dissolution of cassiterite in HI at 100 °C for tin isotope analyses. Hydroiodic acid has not been used widely as it is expensive, easily reacts with oxygen, and has a significantly higher Pb blank than other acids (HI is less stable than other acids and, therefore, difficult to purify). Carr et al. (2020) and Tapster and Bright (2020) used hydrobromic acid (HBr) to decompose cassiterite in a Teflon-lined autoclave at 200 °C. This decomposition procedure has a low Pb blank.

The high precision of ID-TIMS U—Pb dating of cassiterite is offset by the delicate and time-consuming analytical procedure, limited spatial resolution, and the relatively large sample size (Yang et al., 2020, 2021), which hinder the wide application of this method. Instead, the chemical and analytical challenges facilitate the development of in situ U—Pb dating methods applied to cassiterite. Laser ablation-inductively coupled plasma-mass spectrometry (LA-ICP-MS) is a useful method for U—Pb dating of cassiterite. It requires matrix-matched reference materials for correction of instrumental mass fractionation. Yuan et al. (2011) reported the first LA-ICP-MS cassiterite U—Pb age for the Furong tin deposit in South China. The good agreement between LA-ICP-MS and ID-TIMS results of AY-4 cassiterite made it a candidate to serve as a reference material for many follow-up LA-ICP-MS cassiterite U—Pb dating studies (Zhang et al., 2014; Deng et al., 2017; Wang et al., 2017; Zhang et al., 2017; Hu et al., 2020; Zhang et al., 2020). Due to the scarcity of cassiterite reference materials, alternative approaches have been taken for U—Pb dating of cassiterite by LA-ICP-MS using non-matrix-matched reference materials. These non-matrix-matched methods include: (i) Neymark et al. (2018) used the highly repeatable results of "SPG" cassiterite to overcome matrix-matching problems. The difference between the NIST 612 glass normalised biased U—Pb age and Pb—Pb age of "SPG" cassiterite is used to estimate a correction factor for instrumental U—Pb fractionation. This correction factor is then applied to measured U/Pb ratios and Tera-Wasserburg intercept ages. (ii) Cheng et al. (2019) tuned the instrument to keep the ablation of cassiterite and NIST 612 glass produce similar U/Pb downhole fractionation (DHF) patterns during each analytical session, indicating that DHF between cassiterite and NIST 612 glass was not always similar. (iii) Gemmrich et al. (2021) used rutile as primary reference material to calibrate cassiterite. They obtained a systematic offset of nearly 8% for intercept ages in the Tera-Wasserburg diagram. (iv) Chen et al. (2021) adapted the method described by Luo et al. (2018) by adding in some nitrogen and water vapour to the carrier gas to minimize the elemental and isotopic fractionation between different matrices (zircon and cassiterite). Secondary ion mass spectrometry (SIMS) has not been widely applied yet to U—Pb dating of cassiterite. Carr et al. (2017) reported the first SIMS U—Pb cassiterite ages using the Yankee cassiterite as a reference material.

There are only a few established cassiterite reference materials available for in situ U—Pb dating (AY-4, SPG, and Yankee). Among these samples, AY-4 is the most commonly used cassiterite reference material in the world. A new ID-TIMS U—Pb age for cassiterite AY-4, (151.9 ± 2.2 Ma; Carr et al., 2020), however, is nearly 4% younger than the originally reported U—Pb age (158.2 ± 0.4 Ma; Yuan et al., 2011), which may indicate that its age is not homogeneous (Carr et al., 2020). Furthermore, some characterized cassiterite samples (e.g., SPG-IV, Yankee) may not be widely available in the future. Therefore, it is urgent (i) to characterize more cassiterite reference materials for in situ U—Pb age determination and (ii) to assess the age homogeneity of cassiterite reference material AY-4.

The main objectives of this study are (i) to establish a procedure for in situ U—Pb dating of cassiterite by LA-SF-ICP-MS; (ii) to investigate the isobaric interference of tungsten oxides on ^{202}Hg and ^{204}Pb. (iii) to verify the feasibility of the ^{208}Pb correction procedure for common Pb contributions. (iv) to develop cassiterite reference materials suitable for in situ U—Pb dating.

2. Sample location

Cassiterite samples for this study are from tin deposits of Paleoproterozoic to Cretaceous age. Samples were provided by geologists or were purchased from mineral collectors.

2.1. PitAB (Madeira and Água Boa deposits, Pitinga Tin Province, Brazil)

Cassiterite PitAB was sampled from the Madeira and Água Boa A-type tin-bearing granites, Pitinga Tin Province, Brazil, and was described by Neymark et al. (2018). Ore-bearing Madeira and Água Boa A-type granites yield U—Pb zircon ages of 1825 ± 14 Ma and 1831 ± 11 Ma, respectively (Neto et al., 2014). PitAB yields an intercept LA-ICP-MS age of 1827.8 ± 6.3 Ma in the Tera-Wasserburg diagram (Neymark et al., 2018).

2.2. Rond-A (Rondônia tin province, placer tin deposit, Brazil)

This sample was collected from a placer tin deposit in the Rondônia tin province, Brazil, where several 1.60 Ga to 0.97 Ga old rapakivi granite suites intruded Paleo- to Mesoproterozoic medium- to high-grade metamorphic rocks (Bettencourt et al., 1999). Greisen-type tin-polymetallic deposits are associated with 1.08–0.97 Ga late-stage rapakivi-type fluorine-rich peraluminous alkali-feldspar granites (Bettencourt et al., 1999). Sample Rond-A yields an intercept age of 1012.9 ± 5.4 Ma in the Tera-Wasserburg diagram and an inverse Pb—Pb isochron age of 1012 ± 23 Ma (Neymark et al., 2018).

2.3. RG-114 (Maniema province, Democratic Republic of the Congo)

Cassiterite sample RG-114 was collected from the Kalima area, Maniema province, Democratic Republic of the Congo. The deposit consists of quartz veins hosted in the Kalima granite and adjacent Mesoproterozoic metasedimentary rocks (Dewaele et al., 2015). The emplacement of the quartz veins altered the granite and its metasedimentary wall rocks. The ^{40}Ar/^{39}Ar ages of muscovite from a quartz vein and an associated pegmatite indicate that the Kalima area experienced two episodes of hydrothermal activity at ~1020 Ma and ~ 990 Ma (Dewaele et al., 2015).

2.4. Kard (Kekekaerde W—Sn deposit, East Kunlun Orogen, NW China)

Cassiterite sample Kard was collected from the Kekekaerde W—Sn deposit in the Baiganhu W—Sn ore field, East Kunlun Orogen, NW China. In this deposit, cassiterite mainly occurs in quartz veins and greisens and rarely in skarns associated with the granite. Bao et al. (2008) reported a TIMS U—Pb zircon age of 432 ± 1 Ma for the monzogranite suggesting a Middle Silurian age for the intrusion and associated mineralization. Other ages obtained for these rocks include (i) a SIMS U—Pb zircon ages of 421 ± 4 Ma and 422 ± 3 Ma for the monzogranite and potassic granite, respectively (Li et al., 2012), (ii) a LA-ICP-MS U—Pb zircon age of 430.5 ± 1.2 Ma for the monzogranite

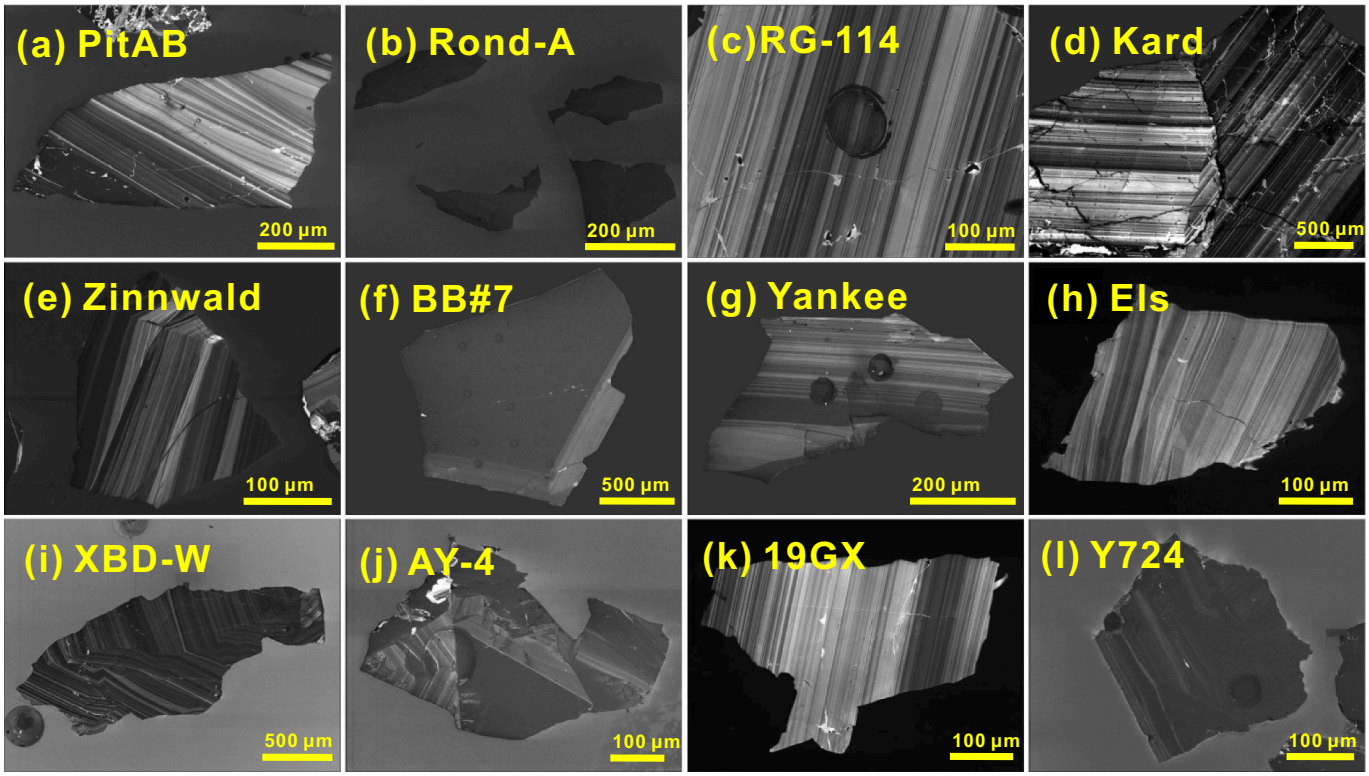

Fig. 1. Representative CL images of cassiterite samples. Samples PitAB, RG-114, Kard, Zinnwald, Yankee, Els, XBD-W, AY-4, and 19GX show oscillatory growth zoning. Samples Rond-A and Y724 do not show growth zoning. Sample BB#7 has a distinctive rim of contrasting composition.

(Gao et al., 2014), and (iii) ID-TIMS and LA-MC-ICP-MS ages of 416 ± 1 Ma and 426 ± 13 Ma, respectively, for cassiterite (Deng et al., 2017).

2.5. Zinnwald (Erzgebirge tin province of eastern Germany and the western Czech Republic)

Cassiterite sample Zinnwald originates from the Cinovec-Zinnwald Li—Sn deposit in the Erzgebirge, which is a major Variscan Sn province at the northern margin of the Bohemian Massif. The Altenberg granite gives an ID-TIMS U—Pb zircon age of 319.2 ± 2.4 Ma (Romer et al., 2010) and molybdenite from Sn deposits of the Eastern Erzgebirge (Sadisdorf, Cinovec-Zinnwald; Krupka) give *Re*—Os ages in the range of 322–315 Ma (Romer et al., 2007; Ackerman et al., 2017). Cassiterite from the Cinovec-Zinnwald Li—Sn deposit yields a common Pb corrected $^{206}Pb/^{238}U$ age of 321.5 ± 3.1 Ma (Zhang et al., 2017).

2.6. BB#7 (Maine, USA)

Cassiterite sample BB#7 was collected from a zoned lithium-cesium-tantalum (LCT) type pegmatite at the BB#7 pegmatite quarry, Oxford County, Maine, USA. Previous studies constrained the age of pegmatites from Maine to range from ~250 Ma to ~290 Ma (Tomascak et al., 1996; Bradley et al., 2016). The Mount Mica pegmatite, which is close to the sample location, yields an ID-TIMS U—Pb zircon age of 263.9 ± 0.2 Ma and an Ar—Ar muscovite age of 259.9 ± 2.3 Ma (Bradley et al., 2016).

2.7. Yankee (Yankee lode, Australia)

Cassiterite sample Yankee was collected from the Yankee lode in the New England Orogen of eastern Australia. Cassiterite occurs in quartz veins associated with the Mole granite that was emplaced at 246 ± 2 Ma (Kleeman et al., 1997). This age was later confirmed by Schaltegger et al. (2005) who reported TIMS U—Pb ages of 247.7 ± 0.5 Ma for magmatic zircon and 244.4 ± 1.4 Ma for hydrothermal monazite. Yankee cassiterite yields an ID-TIMS U—Pb ages of 246.48 ± 0.51 Ma (Carr et al., 2020).

2.8. Els (Elsmore granite, Australia)

Cassiterite sample Els was collected from the Elsmore granite, which is located in the New England Orogen of eastern Australia. The Elsmore granite hosts a significant greisen- and vein-type Sn mineral deposit. Cross and Blevin (2013) reported a SHRIMP zircon U—Pb age of 250.3 ± 1.8 Ma for the Elsmore granite.

2.9. XBD-W (Xuebaoding deposit, Sichuan Province, China)

The Xuebaoding Sn–W–Be polymetallic deposit is located in the Sichuan Province, western China. The Xuebaoding deposit is renowned for euhedral, *gem* quality, coarse grained scheelite, cassiterite, and beryl crystals. There is a wide range of age data available for the Xuebaoding granite and associated mineralization, including $^{40}Ar/^{39}Ar$ ages ranging from 193.7 ± 1.1 Ma to 200.6 ± 1.3 Ma for magmatic muscovite (Liu et al., 2010), a $^{40}Ar/^{39}Ar$ age of 191.8 ± 0.7 Ma for fluid inclusions in quartz (Cao et al., 2002), and a Sm—Nd isochron age for scheelite of 182.0 ± 9.2 Ma (Liu et al., 2007a, 2007b). Cassiterite from this location gave a LA-MC-ICP-MS U—Pb isochron age of 193.6 ± 6.0 Ma, which agrees with the $^{40}Ar/^{39}Ar$ age of muscovite intergrown with cassiterite (194.5 ± 1.0 Ma; Zhang et al., 2014).

2.10. AY-4 (Furong tin deposit, Hunan province, China)

AY-4 cassiterite is one of the most commonly used reference materials for U—Pb dating of cassiterite by LA-ICP-MS (Zhang et al., 2014; Deng et al., 2017; Zhang et al., 2017; Hu et al., 2020; Zhang et al., 2020). This sample was collected from the Furong tin deposit located at the southern margin of the Qitianling granite batholith in southern Hunan,

south China. It was firstly characterized by Yuan et al. (2011), who reported a LA -ICP-MS age of 159.9 ± 1.9 Ma and a ID-TIMS age of 158.2 ± 0.4 Ma. Later U—Pb dating, however, gave younger ages for AY-4 cassiterite. For instance, Carr et al. (2020) presented an ID-TIMS U—Pb age of 151.9 ± 2.2 Ma, which is nearly 4% younger than the originally reported age, and Chen et al. (2021) reported LA-ICP-MS U—Pb ages in the range of 155.3 ± 0.9 Ma to 157.4 ± 0.8 Ma for AY-4 cassiterite.

2.11. 19GX (Shanhu W—Sn deposit, Guangxi Province, China)

Cassiterite sample 19GX was collected from the Shanhu W—Sn deposit in the Nanling Range of South China. This quartz vein-type W—Sn deposit is spatially related to the Yantianling muscovite granite, which has U—Pb zircon ages of 101.0 ± 1.5 Ma and 100.4 ± 1.1 Ma, consistent with the U—Pb cassiterite ages of 100.2 ± 1.0 Ma and 100.5 ± 1.1 Ma (Zhang et al., 2020).

2.12. Y724 (Yinyan porphyry tin deposit, Guangdong Province, China)

The Yinyan porphyry tin deposit is spatially associated with quartz porphyry and granite porphyry and located in the western Guangdong Province, China. Hu et al. (2020) reported U—Pb zircon ages of 78.5 ± 0.4 Ma for the quartz porphyry and 79.2 ± 0.9 Ma for the granite porphyry. Cassiterite sample Y724 has an intercept age of 78.2 ± 0.7 Ma in the Tera-Wasserburg diagram. Zircon and cassiterite U—Pb ages agree well with *Re*—Os molybdenite ages of 78.8 ± 2.6 Ma (Zheng et al., 2016) and 77.0 ± 0.5 Ma (Hu et al., 2020).

3. Analytical techniques

All cassiterite grains were concentrated using a Frantz magnetic separator and heavy liquids and selected by hand picking under a binocular microscope. For each sample, some cassiterite grains were embedded in a 1-in. epoxy mount, sectioned to expose their interior, polished, and mapped by optical microscopy. The texture of cassiterite crystals was characterized by cathodoluminescence (CL) imaging. The chemical homogeneity was examined by element mapping using laser ablation quadrupole ICP-MS (LA-Q-ICP-MS) analysis. The U—Pb isotopic homogeneity of cassiterite was tested by laser ablation sector field ICP-MS (LA-SF-ICP-MS) analysis. Relatively homogeneous samples (six in total) with low common Pb were selected for U—Pb ID-TIMS analysis.

3.1. CL imaging

Cathodoluminescence (CL) images of cassiterite were acquired on a MIRA 3 XMU (TESCAN) equipped with a panchromatic CL detector (350–650 nm) (TESCAN BSE/CL detector) and operated under high vacuum mode with carbon coat at Beijing Kuangyan Geoanalysis Laboratory Co., Ltd. Representative CL images are shown in Fig. 1.

3.2. LA-Q-ICP-MS element mapping

LA-Q-ICP-MS element mapping was conducted at the Institute of Geology and Geophysics, Chinese Academy of Sciences (IGGCAS). All cassiterite samples were mounted and polished in 2.5 cm-diameter epoxy mounts. These mounts were placed into the HelEx-II ablation cell for trace element screening (^{24}Mg, ^{29}Si, ^{43}Ca, ^{45}Sc, ^{49}Ti, ^{55}Mn, ^{57}Fe, ^{63}Cu, ^{66}Zn, ^{89}Y, ^{90}Zr, ^{93}Nb, ^{115}In, ^{177}Hf, ^{181}Ta, ^{182}W, ^{204}Pb, ^{206}Pb, ^{207}Pb, ^{208}Pb, ^{232}Th, ^{238}U) using a Photo Machine Analyte G2 193 nm ultraviolet (UV) ArF-Excimer laser ablation system (Teledyne CETAC) coupled to an Agilent 7500a Q-ICP-MS (Agilent Technologies). The laser repetition rate and fluence were set to 20 Hz and 2.0 J cm^{-2}, respectively. The laser spot was 30 μm in diameter and the line scan speed was 30 μm/s. NIST SRM 614 (Jochum et al., 2011) and ARM-3 (Synthetic glass, Wu et al., 2019) were employed as reference materials for quantification of element concentrations. Concentration data were reduced using the Iolite software with the "Trace_Element" DRS and a "semi quantitative" (i.e., by comparing the signal intensity with NIST ARM 614 rather than using internal standard) standardisation method. Because of the matrix difference between the NIST 614 glass and cassiterite, the measured Pb, Th and U concentrations are not better than ±20%. 2D element images were generated using the Iolite software v4 (Paul et al., 2012; Petrus et al., 2017). Detailed instrument settings are summarized in Table 1.

Table 1
Typical instrumental parameters of LA-(Q, SF)-ICP-MS for element imaging and U—Pb dating.

	U-Pb dating	Element Mapping
Laser ablation systems		
Manufacturer, model & type	Coherent Geolas HD	Photon Machine Analyte G2
Ablation cell & volume	In-house built cell, aerosol dispersion volume < 3 cm^3	HelEx ablation cell
Laser wavelength	193 nm	193 nm
Energy density/ fluence	~ 4 J/cm^2	~ 2 J/cm^2
Repetition rate	5 Hz	20 Hz
Used spot size	32–44 μm	30 μm
Sampling mode/ pattern	Single hole drilling, five cleaning pulses	Line scanning with a speed of 30 μm/s
Ablation gas flow	~ 0.75 L min^{-1} (He)	~ 0.75 L min^{-1} (He)
Ablation duration	variable	30 s
ICP-MS		
Manufacturer, model & type	Thermo Fisher Scientific Element XR	Agilent 7500a
RF Power	1320 W	1350 W
Guard electrode	Connected (Pt)	Disconnected (Pt)
Sample cone	Nickel Jet sample cone	Nickel
Skimmer cone	Nickel X skimmer cone	Nickel
Carrier gas flow (Ar)	0.95 L min^{-1}	1.15 L min^{-1}
Enhancement gas flow (N_2)	6 mL min^{-1}	No
Scan mode	E-scan	Peak jump
Isotopes measured (m/z) + sample time	^{202}Hg (2 ms), ^{204}Pb (2 ms), ^{206}Pb (15 ms), ^{207}Pb (30 ms), ^{208}Pb (10 ms), ^{232}Th (10 ms), ^{235}U (10 ms), ^{238}U (15 ms)	^{24}Mg, ^{29}Si, ^{43}Ca, ^{45}Sc, ^{49}Ti, ^{55}Mn, ^{57}Fe, ^{63}Cu, ^{66}Zn, ^{89}Y, ^{90}Zr, ^{93}Nb, ^{115}In, ^{177}Hf, ^{181}Ta, and ^{182}W all 6 ms; ^{204}Pb, ^{206}Pb, ^{207}Pb, ^{208}Pb, ^{232}Th, and ^{238}U all 10 ms.
Mass window	20%	–
Sample per peak	20	–
Detection system	Single SEM detector in triple mode, Counting, Analog and Faraday	Single SEM in double mode, Counting and Analog
Resolution	Low (~300)	~300
Total integration time per reading	0.27 s	0.30 s

3.3. ID-TIMS U—Pb analysis

Among the cassiterite samples analysed by LA-ICP-MS, a few samples were selected for ID-TIMS U—Pb analysis. Preference was given to cassiterite samples that had been dated by ID-TIMS method before. Cassiterite AY-4 is was selected as available ID-TIMS ages differ beyond analytical uncertainties. Samples with relatively high common Pb contents were not selected for ID-TIMS analysis. Among several cassiterite samples within the same age range, we only chose for ID-TIMS analysis.

Six cassiterite samples were analysed at GFZ German Research Centre for Geosciences, Potsdam. Previous studies showed that acid cleaning or leaching of cassiterite removes considerable amounts of common Pb hosted in sulphides and silicates (Gulson and Jones, 1992; Tapster and Bright, 2020). To remove intergrowths and inclusions of minerals that can carry common Pb, all cassiterite samples were ground in an agate mortar and then leached in 22 mol L^{-1} distilled HF (2 days on

Table 2
ID-TIMS U—Pb analytical results for cassiterite.

Sample [a]	Weight	Concentrations		^{206}Pb	Common	Atomic ratios [c]							Apparent ages (Ma) [d]					
	(mg)	(μg g^{-1})		$/^{204}Pb$	lead	^{206}Pb		^{207}Pb		Rho	^{207}Pb			^{206}Pb		^{207}Pb		^{207}Pb	
		U	Pb	Measured ratios [b]	(μg g^{-1})	$/^{238}U$	2σ	$/^{235}U$	2σ		$/^{206}Pb$	2σ		$/^{238}U$		$/^{235}U$		$/^{206}Pb$	
PitAB, Madeira and Água Boa deposits, Pitinga Tin Province, Brazil																			
Initial Pb [e]: $^{206}Pb/^{204}Pb = 15.8 \pm 0.5$, $^{207}Pb/^{204}Pb = 15.4 \pm 0.15$, $^{208}Pb/^{204}Pb = 36.0 \pm 1.0$																			
C1–1	1.8	2.2	1.2	112.5	0.5	0.3286	0.0022	5.076	0.081	0.18	0.1120	0.0018		1832	11	1832	14	1833	29
C1–2	3.2	2.1	1.0	118.1	0.4	0.3297	0.0024	5.138	0.085	0.29	0.1130	0.0018		1837	11	1842	14	1849	29
C1–3	1.4	1.9	1.0	98.6	0.4	0.3292	0.0033	5.109	0.068	0.38	0.1126	0.0022		1835	16	1838	18	1841	36
C1–4	5.7	2.0	1.0	140.6	0.3	0.3305	0.0018	5.123	0.064	0.24	0.1124	0.0014		1841	9	1840	11	1839	22
C1–5	2.4	1.8	1.0	98.8	0.5	0.3286	0.0027	5.091	0.094	0.21	0.1124	0.0021		1832	13	1835	16	1838	34
Rond-A, Rondônia tin province, placer tin deposit, Brazil																			
Initial Pb [e]: $^{206}Pb/^{204}Pb = 19.9 \pm 0.5$, $^{207}Pb/^{204}Pb = 15.4 \pm 0.15$, $^{208}Pb/^{204}Pb = 38.0 \pm 1.0$																			
C2–1	1.2	1.8	0.8	63.2	0.5	0.1700	0.0023	1.720	0.076	0.16	0.0734	0.0033		1012	13	1016	29	1025	90
C2–2	1.6	1.8	0.6	84.9	0.3	0.1720	0.0017	1.753	0.074	0.19	0.0739	0.0031		1023	9	1028	27	1039	84
C2–3	2.1	1.7	0.7	70.0	0.4	0.1722	0.0020	1.723	0.086	0.12	0.0726	0.0036		1024	11	1017	32	1003	101
C2–4	2.0	1.5	0.4	174.7	0.1	0.1720	0.0013	1.743	0.049	0.39	0.0735	0.0019		1023	7	1025	18	1027	52
C2–5	1.3	1.6	1.2	40.4	1.0	0.1730	0.0045	1.719	0.201	0.05	0.0880	0.0092		1026	25	1016	75	989	243
RG-114, Maniema province, Democratic Republic of the Congo																			
Initial Pb [e]: $^{206}Pb/^{204}Pb = 18.0 \pm 0.5$, $^{207}Pb/^{204}Pb = 15.6 \pm 0.15$, $^{208}Pb/^{204}Pb = 38.0 \pm 1.0$																			
C3–1	2.0	1.5	0.4	114.6	0.2	0.1715	0.0011	1.721	0.044	0.16	0.0728	0.0018		1020	6	1016	16	1008	51
C3–2	5.9	1.4	0.3	156.3	0.1	0.1719	0.0010	1.686	0.034	0.28	0.0712	0.0014		1022	5	1003	13	962	40
C3–3	1.8	1.5	0.4	120.9	0.2	0.1720	0.0016	1.716	0.057	0.32	0.0724	0.0023		1023	9	1014	21	996	64
C3–4	2.2	1.4	0.6	60.7	0.4	0.1711	0.0025	1.725	0.097	0.19	0.0731	0.0041		1018	14	1018	36	1017	113
C3–5	7.1	1.2	0.4	86.2	0.2	0.1729	0.0014	1.693	0.059	0.11	0.0710	0.0025		1028	8	1006	22	958	71
C3–6	6.5	1.4	0.4	87.4	0.2	0.1715	0.0019	1.676	0.062	0.26	0.0709	0.0025		1020	11	999	24	954	74
BB#7, Maine, the United States																			
Initial Pb [e]: $^{206}Pb/^{204}Pb = 18.9 \pm 0.5$, $^{207}Pb/^{204}Pb = 15.6 \pm 0.15$, $^{208}Pb/^{204}Pb = 38.0 \pm 1.0$																			
C4–1	1.6	9.6	0.8	85.6	0.4	0.0416	0.0004	0.290	0.015	0.08	0.0505	0.0026		262.8	2.3	258.3	11.6	217	121
C4–2	2.2	7.3	0.5	152.1	0.2	0.0411	0.0003	0.295	0.014	0.50	0.0520	0.0023		259.4	2.2	262.3	11.2	287	103
C4–3	1.8	9.9	0.5	244.7	0.1	0.0415	0.0003	0.295	0.006	0.35	0.0515	0.0010		262.2	1.6	262.1	4.8	261	45
C4–4	1.8	6.2	0.8	52.6	0.6	0.0411	0.0007	0.289	0.031	0.06	0.0509	0.0055		259.9	4.4	257.6	24.4	237	240
C4–5	3.9	8.2	0.6	126.9	0.3	0.0415	0.0007	0.292	0.029	0.70	0.0510	0.0046		262.1	4.1	260.2	22.9	241	210
C4–6	2.3	7.4	0.6	92.3	0.3	0.0416	0.0004	0.295	0.017	0.20	0.0514	0.0029		262.6	2.5	262.1	13.4	257	131
AY-4, Furong tin deposit, Hunan province, China																			
Initial Pb [e]: $^{206}Pb/^{204}Pb = 18.9 \pm 0.5$, $^{207}Pb/^{204}Pb = 15.7 \pm 0.15$, $^{208}Pb/^{204}Pb = 38.0 \pm 1.0$																			
C5–1	1.5	71.8	6.4	42.1	4.8	0.0243	0.0006	0.166	0.021	0.21	0.0497	0.0060		154.5	3.5	156.1	17.9	180	225
C5–2	3.4	18.1	0.9	79.1	0.5	0.0242	0.0002	0.164	0.007	0.17	0.0491	0.0021		153.9	1.5	153.9	6.2	155	101
C5–3	3.1	14.7	0.7	81.7	0.4	0.0243	0.0002	0.163	0.007	0.20	0.0487	0.0021		154.6	1.5	153.4	6.4	135	104
C5–4	3.8	10.4	0.7	50.6	0.5	0.0242	0.0004	0.164	0.014	0.14	0.0493	0.0042		154.2	2.5	154.6	12.4	161	180
C5–5	2.2	31.9	1.8	62.2	1.1	0.0242	0.0003	0.166	0.009	0.07	0.0497	0.0026		154.0	1.9	155.6	7.4	181	122
C5–6	1.4	55.3	2.9	70.2	1.7	0.0243	0.0003	0.165	0.007	0.09	0.0492	0.0022		154.6	1.6	154.8	6.4	158	105
19-GX, Shanhu W—Sn deposit, Guangxi Province, China																			
Initial Pb [e]: $^{206}Pb/^{204}Pb = 18.6 \pm 0.5$, $^{207}Pb/^{204}Pb = 15.6 \pm 0.15$, $^{208}Pb/^{204}Pb = 38.0 \pm 1.0$																			
C6–1	1.2	7.6	0.2	131.2	0.1	0.0156	0.0001	0.106	0.005	0.26	0.0492	0.0024		100.0	0.6	102.3	4.8	156	113
C6–2	3.7	9.9	0.3	95.9	0.1	0.0157	0.0001	0.104	0.005	0.25	0.0483	0.0023		100.1	0.8	100.8	4.7	116	112
C6–3	3.0	10.1	0.2	122.2	0.1	0.0156	0.0001	0.100	0.005	0.24	0.0439	0.0018		99.7	0.7	96.5	4.8	–	–
C6–4	1.0	13.0	0.3	161.6	0.1	0.0156	0.0001	0.101	0.003	0.22	0.0471	0.0014		100.0	0.5	98.1	2.8	52	66
C6–5	1.7	10.3	0.3	73.3	0.2	0.0156	0.0002	0.102	0.006	0.15	0.0471	0.0026		100.0	1.0	98.2	5.3	55	97
BB#7 [f], Maine, the United States																			
Initial Pb estimated according to Stacey and Kramers (1975) model																			

(*continued on next page*)

Table 2 (*continued*)

Sample [a]	Weight	Concentrations		^{206}Pb		Common	Atomic ratios [c]						Apparent ages (Ma) [d]					
	(mg)	(μg g^{-1})		/^{204}Pb		lead	^{206}Pb		^{207}Pb		Rho	^{207}Pb			^{206}Pb		^{207}Pb	
		U	Pb	Measured ratios [b]		(μg g^{-1})	/^{238}U	2σ	/^{235}U	2σ		/^{206}Pb	2σ		/^{238}U		/^{235}U		/^{206}Pb	
T1	4.6	13.0	0.6	231.6		0.1	0.0419	0.0004	0.298	0.004	0.72	0.0516	0.0005		264.7	4.5	265.0	7.9	268	49
T2	2.9	14.5	0.8	155.4		0.0	0.0416	0.0003	0.296	0.006	0.67	0.0515	0.0008		262.8	4.1	262.9	10.9	264	76
T3	0.8	12.2	1.8	41.1		0.0	0.0411	0.0010	0.292	0.037	0.86	0.0515	0.0055		259.6	12	260.2	65.6	265	495
T4	8.1	14.8	0.7	333.3		0.1	0.0418	0.0003	0.297	0.003	0.79	0.0515	0.0004		263.7	4.1	263.9	5.9	265	32
T5	1.8	19.4	1.3	102.0		0.0	0.0419	0.0004	0.296	0.010	0.67	0.0513	0.0013		264.3	5.6	263.4	17.0	255	121
T6	1.9	21.9	1.5	96.3		0.0	0.0418	0.0005	0.296	0.010	0.68	0.0514	0.0015		263.9	5.9	263.5	18.5	259	131
T7	1.0	18.6	2.2	48.6		0.0	0.0417	0.0008	0.296	0.026	0.79	0.0515	0.0039		263.3	9.8	263.4	46.7	264	345
T8	2.0	13.3	1.5	49.1		0.1	0.0410	0.0008	0.291	0.027	0.76	0.0515	0.0040		258.8	10	259.4	47.3	265	357
T9	1.1	11.7	1.3	47.9		0.0	0.0416	0.0007	0.295	0.026	0.82	0.0514	0.0038		262.8	8.7	262.4	45.6	259	341
T10	5.7	15.8	0.8	223.0		0.0	0.0418	0.0002	0.297	0.004	0.67	0.0516	0.0006		263.9	3.0	264.2	7.2	267	49

[a] Small fragments from single cassiterite crystals. Fragments were selected to show only fresh fracture surfaces.

[b] Lead isotope ratios corrected for fractionation, blank and isotopic tracer. Sample PitAB, Rond-A, RG-114, BB#7, AY-4, and 19GX were analysed at GFZ German Research Centre for Geosciences, Potsdam, Germany, using a ^{205}Pb—^{235}U mixed isotopic tracer. Total blanks were less than 15 pg for lead and less than 1 pg for uranium. Sample BB#7 was also analysed at Tianjin Institute of Geology and Mineral Resources, China. Total blanks were less than 25–92 pg for lead and less than 4–12 pg for uranium.

[c] Lead corrected for fractionation, blank, isotopic tracer, and initial lead.

[d] Apparent ages were calculated using the constants of Jaffey et al. (1971) recommended by IUGS. $\lambda^{238} = 1.55125$ E-10 y^{-1}, $\lambda^{235} = 9.848$ E-10 y^{-1}.

[e] Initial lead was estimated using the $^{207}Pb/^{204}Pb$ vs. $^{206}Pb/^{204}Pb$ diagram.

[f] Initial lead was estimated using Stacey and Kramers (1975) model.

hotplate at 140 °C), 6 mol L^{-1} distilled HCl (2 days on hotplate at 140 °C), 7 mol L^{-1} distilled HNO_3 (1 day on hotplate at 140 °C). After the leaching, we rinsed the samples with distilled H_2O and distilled acetone twice.

For cassiterite digestion, we used concentrated HBr acid as described by Carr et al. (2020) and Tapster and Bright (2020). A mixed ^{205}Pb—^{235}U tracer was added and dried before sample dissolution. Approximately 1 mL of 9 mol L^{-1} HBr was added to each beaker. The beakers were placed inside clean Teflon liners (three vials per liner) with 1 mL of 9 mol L^{-1}HBr acid added to the liner base, and then sealed in Parr vessels and placed in an oven at 210 °C for approximately 10 days. Commonly, cassiterite was dissolved completely. After cassiterite decomposition, the solution was dried on a hotplate at 80 °C and then converted to chloride by adding 0.5 mL of 6 mol L^{-1} HCl and taken to dryness at 80 °C. The U and Pb were separated using the HBr-HCl ion-exchange procedure described in Romer and Lüders (2006). U and Pb were loaded with H_3PO_4 and silica gel on the same Re filament. The isotopic ratios of U and Pb were measured using a Triton TIMS instrument operated in static or dynamic multi-collection mode using Faraday collectors and an ion counter, depending on signal intensity. Lead was analysed at 1200–1260 °C and U at 1360–1430 °C. Data reduction followed the procedures described by Schmid et al. (2003). The procedural blank for Pb and U are better than 15 pg and 1 pg, respectively.

Sample BB#7 was also analysed at Tianjin Institute of Geology and Mineral Resources, China and following the procedures described by Yuan et al. (2008, 2011). Cassiterite was firstly pulverized (< 30 μm) and then rinsed with H_2O and ethanol. The samples were sequentially cleaned using 6 mol L^{-1} HCl (1–2 h at 70 °C) and a mixture of 7 mol L^{-1} HNO_3 and 6 mol L^{-1} HCl (1–2 h at 70 °C). Then, the samples were rinsed with H_2O and ethanol. Sample aliquots were digested using 2–3 mL 12 mol L^{-1} HCl in sealed Parr autoclaves at 210 °C for at least 72 h. The digested samples were split by weight. A mixed ^{208}Pb—^{235}U tracer was added to one split to precisely measure the U and Pb content. The second split was used to measure the Pb isotope ratios. The separation of U and Pb was adapted from the analytical procedure described in Yuan et al. (2008, 2011). Uranium and Pb were loaded with H_3PO_4 and silica gel onto Re filaments. The isotopic ratios of U and Pb were measured using a Triton TIMS instrument with Pb isotope ratios measured at 1250–1350 °C and U isotope ratio measured at 1350–1450 °C. Total procedure blanks during this study were 25–92 pg for Pb and 4–12 pg for U.

Pb/U ratios corrected for fractionation, common Pb in the spike, initial common Pb, and Pb and U blank. All uncertainties were estimated using a Monte-Carlo simulation with the following uncertainties: measurement uncertainties, 30% uncertainty for the correction of mass fractionation, 50% uncertainty for the amount of Pb and U blank and 0.5, 0.15 and 0.5 absolute uncertainty for $^{206}Pb/^{204}Pb$, $^{207}Pb/^{204}Pb$ and $^{208}Pb/^{204}Pb$ of the blank and initial Pb composition, respectively. Decay constants are those of Jaffey et al. (1971): ^{238}U and ^{235}U are 1.55125 × 10^{-10} y^{-1} and 9.8485 × 10^{-10} y^{-1}. The initial $^{206}Pb/^{204}Pb$ and $^{207}Pb/^{204}Pb$ values (listed in Table 2) were estimated using the $^{206}Pb/^{204}Pb$ vs. $^{238}U/^{204}Pb$ and $^{207}Pb/^{204}Pb$ vs. $^{206}Pb/^{204}Pb$ diagrams, respectively. All age errors quoted in the text and in Table 2 and error ellipses shown in concordia diagrams are given at the 95% confidence level. The data were plotted using Isoplot 3.0 (Ludwig, 2003).

3.4. LA-SF-ICP-MS U—Pb analysis

In situ U—Pb isotope measurements were performed using a single collector SF-ICP-MS instrument (Element XR, Thermo-Fisher) and a 193 nm ArF excimer laser (Geolas HD, Coherent), located at the IGGCAS. The Element XR instrument is equipped with a high-capacity vacuum pump (OnTool Booster 150, Asslar, Germany), with which the high-performance Jet sample cone allowed for a dramatic increase of the signal intensity. Helium (~0.75 L min^{-1}) and a little nitrogen (6 mL/min) were used as carrier gas through the ablation cell and mixed with

Table 3
Compilation of LA-SF-ICP-MS U—Pb dating results of cassiterite.

Cassiterite	n	Pb	Th	U	$^{238}U/^{206}Pb$		$^{207}Pb/^{206}Pb$		$^{207}Pb/^{235}U$		$^{206}Pb/^{238}U$		$^{208}Pb/^{206}Pb$		f_{206} [a] (%)		^{207}Corr. age		^{208}Corr. age		ID-TIMS
					Mean	2SD	Mean	2SD	Mean	2SD	Mean	2SD	Mean	2SD	Mean	2SD	$^{206}Pb/^{238}U$		$^{206}Pb/^{238}U$		
		μg g^{-1}															Mean	2SD	Mean	2SD	
PitAB	22	3.64	0.016	8.7	2.95	0.28	0.1380	0.0689	6.5060	3.9045	0.3397	0.0357	0.0713	0.1942	3.15	8.57	1833	53	1830	25	1840(13)
Rond-A	24	0.91	0.009	5.0	5.72	0.54	0.0867	0.0714	2.0607	1.9348	0.1754	0.0206	0.0372	0.1731	1.73	8.03	1024	25	1023	25	1022(5)
RG-114	24	0.54	0.003	3.5	5.79	0.28	0.0839	0.0269	1.9898	0.9170	0.1728	0.0084	0.0227	0.0556	1.05	2.58	1015	33	1017	38	1022(3)
Kard	21	0.37	0.006	5.5	14.33	0.99	0.0663	0.0328	0.6148	0.3332	0.0699	0.0050	0.0354	0.0965	1.69	4.60	429.5	15.9	428.0	14.0	
Zinnwald	22	0.34	0.004	6.6	19.26	0.67	0.0628	0.0313	0.4286	0.1922	0.0519	0.0018	0.0295	0.0614	1.41	2.94	322.3	11.4	321.8	8.7	
BB#7	23	1.00	0.002	24.1	23.98	0.78	0.0529	0.0096	0.3106	0.0616	0.0417	0.0014	0.0177	0.0298	0.85	1.43	262.9	7.8	261.2	6.8	262.7(0.9)
Yankee	24	0.70	0.019	17.7	23.66	4.18	0.1088	0.1121	0.6400	0.7912	0.0426	0.0083	0.1609	0.3181	7.72	15.3	248.4	8.9	246.8	6.4	246.5(0.5)[b]
Elsmore	24	0.25	0.003	6.4	25.65	1.27	0.0587	0.0145	0.2792	0.0575	0.0390	0.0019	0.0270	0.0481	1.29	2.31	244.4	13.0	243.5	8.5	
XBD-W	17	0.06	0.001	1.5	29.80	3.83	0.1007	0.0866	0.4643	0.5049	0.0337	0.0047	0.1663	0.2403	8.00	11.6	199.6	4.9	196.1	5.2	
AY-4	30	1.56	0.000	71.3	39.93	2.04	0.0690	0.0378	0.2394	0.1467	0.0251	0.0013	0.0655	0.0937	3.16	4.51	155.5	1.2	154.5	2.7	154.3(0.7)
19GX	21	0.39	0.008	26.2	63.22	2.60	0.0541	0.0235	0.1137	0.0532	0.0158	0.0007	0.0243	0.0803	1.17	3.88	100.4	2.5	100.0	1.8	100.0(0.3)
Y724	24	2.96	0.132	223	79.36	7.99	0.0714	0.0606	0.1242	0.1262	0.0126	0.0013	0.0760	0.1593	3.67	7.69	78.4	3.2	77.8	3.2	

[a] f_{206}, common ^{206}Pb in total ^{206}Pb; f_{206} = [(^{208}Pb/^{206}Pb) measured - (^{208}Pb/^{206}Pb) radiogenic]/ [(^{208}Pb/^{206}Pb) common - (^{208}Pb/^{206}Pb) radiogenic].
[b] ID-TIMS age: ID-TIMS age of Yankee cassiterite is from Carr et al. (2020), other cassiterite ages are from this study.

argon (0.95 L min^{-1}) downstream of the ablation cell to achieve high sensitivity for U and Pb isotopes. For instrumentation details see Wu et al. (2020). Daily optimization of instrument performance using NIST SRM 614 and ARM-3 reference materials involved maximising the signal to background intensity ratios for Pb, Th, and U, while keeping oxide production rates ($ThO^+/Th^+ < 0.5\%$) and double-charged ions ($Ca^{2+}/Ca^+ < 1.0\%$) low and maintaining stable plasma conditions (U^+/Th^+ in the range of 0.95–1.05). The isotopes ^{202}Hg, ^{204}Pb, ^{206}Pb, ^{207}Pb, ^{208}Pb, ^{232}Th, ^{235}U, and ^{238}U were measured by cycling the electrostatic analyser in the *E*-Scan mode at a static magnetic mass. The dwell time was set to 15 ms for ^{206}Pb and ^{238}U, 2 ms for ^{202}Hg and ^{204}Pb, 10 ms for ^{208}Pb and ^{232}Th, and 30 ms for ^{207}Pb. Typical operating conditions are presented in Table 1. Prior to each analytical session, a pre-ablation run was used to remove any contamination from the cassiterite surface by ablating a 90 μm spot for 5 pulses. Each spot analysis included approximately 15 s background and 45 s sample data acquisition.

The raw data (sequence of calibration materials and samples, as well as the intensities of all isotopes of all scans) were exported for offline data reduction using Iolite software with the "Trace_Element" DRS and the "semi quantitative" standardisation method for calculation of trace element contents (Paton et al., 2011) and Glitter software for U—Pb age calculation (Griffin et al., 2008). Signals of ^{204}Pb, ^{206}Pb, ^{207}Pb, ^{208}Pb, ^{232}Th, and ^{238}U were acquired for U—Pb dating, whereas the ^{235}U signal was calculated from ^{238}U based on the ratio $^{238}U/^{235}U = 137.88$. SPG-II cassiterite with a known ID-TIMS age of 1539.5 ± 0.9 Ma (Rizvanova and Kuznetsov, 2020), used as a primary U—Pb reference material, showed systematic elemental fractionation allowing for downhole fractionation correction. We analysed BB#7 or Y724 cassiterite as secondary reference materials to monitor data reproducibility.

For low Th phases like rutile and cassiterite, common Pb can be accurately corrected by measuring ^{208}Pb (Zack et al., 2011). Because of the low ^{232}Th contents of cassiterite, radiogenic ^{208}Pb, which is derived from the radioactive decay of ^{232}Th, is minor or negligible in cassiterite. Furthermore, ^{208}Pb is the most abundant common Pb isotope and does not have interferences of Hg and W-oxides, which hamper the analysis of ^{204}Pb. Therefore, cassiterite is a very good candidate for the ^{208}Pb correction method. Cassiterite ^{208}Pb/^{206}Pb ratios were calculated offline and calibrated against NIST SRM 612. The common ^{206}Pb proportion (f_{206}) is calculated from:

$$f_{206} = \left[\left(^{208}Pb/^{206}Pb\right)_{measured} - \left(^{208}Pb/^{206}Pb\right)_{rad}\right] \Big/ \left[\left(^{208}Pb/^{206}Pb\right)_{common} - \left(^{208}Pb/^{206}Pb\right)_{rad}\right] \quad (1)$$

and

$$\left(^{208}Pb/^{206}Pb\right)_{rad} = \left(^{232}Th/^{238}U\right) * \left[\left(e^{\lambda 232t} - 1\right)/\left(e^{\lambda 238t} - 1\right)\right] \quad (2)$$

$(^{208}Pb/^{206}Pb)_{common}$ is estimated using the two-stage crustal Pb model of Stacey and Kramers (1975). All cassiterite age data are presented in two different ways: (1) uncorrected data are reported as intercept ages in the Tera-Wasserburg diagram. All intercept ages in this study are anchored with ^{207}Pb/^{206}Pb ratios derived from the Stacey and Kramers (1975) Pb model with an uncertainty at the 2% level unless otherwise stated. In addition, weighted ^{206}Pb/^{238}U mean ages were calculated using the ^{207}Pb correction of common Pb. (2) Data corrected for common Pb using the ^{208}Pb correction are reported in the concordia diagram along with the corresponding weighted ^{206}Pb/^{238}U mean dates.

4. Results

4.1. Samples studied by ID-TIMS and LA-SF-ICP-MS

4.1.1. PitAB (Brazil)

Five fractions of cassiterite sample PitAB have been analysed by ID-TIMS. The individual fractions have ^{206}Pb/^{204}Pb ratios in the range of

98.6 and 140.6. Total Pb contents vary from 1.0 to 1.2 μg g^{-1} and U contents vary from 1.8 to 2.2 μg g^{-1} (Table 2). The five aliquots are concordant and overlap with each other in the Wetherill diagram (Fig. 3a). The corrected apparent $^{207}Pb/^{206}Pb$ age ranges from 1833 ± 29 Ma to 1849 ± 29 Ma and the $^{206}Pb/^{238}U$ age ranges from 1832 ± 11 Ma to 1841 ± 9 Ma. The analysed five aliquots constrain a corrected concordia age of 1837 ± 3 Ma (2 s, MSWD = 0.4). They have corrected weighted average $^{207}Pb/^{206}Pb$ and $^{206}Pb/^{238}U$ ages of 1840 ± 13 Ma (2 s, MSWD = 0.2) and 1836 ± 5 Ma (2 s, MSWD = 0.6), respectively.

Cassiterite sample PitAB shows clear growth zoning, but no signs of alteration in CL images (Fig. 1a). LA-ICP-MS analyses yield U contents in the range from 2.8 to 34.8 μg g^{-1} and the measured common ^{206}Pb fractions (f_{206}) range from 0.01% to 17.17% (Table 3). In Fig. 4a, 22 analyses yield an intercept age of 1833 ± 24 Ma (2 s, MSWD = 0.2) in the Tera-Wasserburg diagram and a ^{207}Pb-corrected $^{206}Pb/^{238}U$ age of 1832 ± 24 Ma. The common Pb corrected data (using the ^{208}Pb-correction) yield a concordia age of 1828 ± 22 Ma (2 s, MSWD = 0.1) and a ^{208}Pb-corrected weighted mean $^{206}Pb/^{238}U$ age of 1829 ± 28 Ma (Fig. 4b). Both common Pb corrected ages and the intercept age from the Tera-Wasserburg diagram using measured data are identical within uncertainty. Furthermore, the LA-ICP-MS and the ID-TIMS ages are consistent within analytical uncertainties. Our LA-ICP-MS and ID-TIMS ages agree well with earlier reported LA-ICP-MS ages (1827.8 ± 6.3 Ma, Neymark et al., 2018).

4.1.2. Rond-A (Brazil)

Five fractions of Rond-A cassiterite have been analysed by ID-TIMS. The measured $^{206}Pb/^{204}Pb$ ratios of sample Rond-A fall in the range of 40.4 and 174.7. Total Pb and U contents range from 0.4 to 1.2 μg g^{-1} and 1.5 to 1.8 μg g^{-1}, respectively (Table 2). The U—Pb results overlap within analytical uncertainty and give a corrected concordia age of 1022 ± 5 Ma (2 s, MSWD = 0.1; Fig. 3b) and a corrected weighted average $^{206}Pb/^{238}U$ age of 1022 ± 5 Ma (2 s, MSWD = 0.8). The corrected weighted average $^{207}Pb/^{206}Pb$ age (1025 ± 36 Ma; 2 s, MSWD = 0.1) has a relatively large uncertainty. Therefore, the best ID-TIMS age estimate for cassiterite sample Rond-A is 1022 ± 5 Ma (the corrected weighted average $^{206}Pb/^{238}U$ age).

The CL images of Rond-A grains show no internal features (Fig. 1b). Twenty-four LA-SF-ICP-MS analyses of cassiterite sample Rond-A constrain an intercept age of 1025 ± 13 Ma (2 s, MSWD = 0.2) in the Tera-Wasserburg diagram, with f_{206} and U ranging from 0.03% to 19.97% and 2.6 to 6.8 μg g^{-1}, respectively (Table 3). The ^{207}Pb-corrected $^{206}Pb/^{238}U$ age is 1024 ± 13 Ma (Fig. 4c). This result agrees well with the common Pb corrected concordia age of 1022 ± 12 Ma (2 s, MSWD = 1.5) and the ^{208}Pb-corrected weighted mean $^{206}Pb/^{238}U$ age of 1023 ± 14 Ma (Fig. 4d). Both common Pb corrected ages and intercept age from Tera-Wasserburg diagram using measured LA-SF-ICP-MS data agree well with our ID-TIMS ages. Our laser ablation and ID-TIMS ages are slightly older (~1% deviation) than reported LA-ICP-MS ages (1012 ± 23 Ma) by Neymark et al. (2018), but they all overlap within uncertainty.

4.1.3. RG-114 (Democratic Republic of the Congo)

The measured total Pb and U contents of cassiterite sample RG-114 range from 0.3 to 0.6 μg g^{-1} and 1.2 to 1.5 μg g^{-1}, respectively (Table 2). The $^{206}Pb/^{204}Pb$ ratios fall in the range of 60.7 and 156.3 and the corrected apparent $^{206}Pb/^{238}U$ ages range from 1018 ± 14 Ma to 1028 ± 8 Ma. Due to the low signal intensity for ^{207}Pb, the $^{207}Pb/^{206}Pb$ ages have relatively large uncertainties and range from 954 ± 74 Ma and 1017 ± 113 Ma. Not all aliquots of RG-114 are concordant, but they are very close to the concordia line and overlap with each other. Six aliquots yield a corrected concordia age of 1021 ± 3 Ma (2 s, MSWD = 13), a corrected weighted average $^{207}Pb/^{206}Pb$ age of 978 ± 24 Ma (2 s, MSWD = 0.7), and a weighted average $^{206}Pb/^{238}U$ age of 1022 ± 3 Ma (2 s, MSWD = 0.6). We consider the corrected mean $^{206}Pb/^{238}U$ age of 1022 ± 3 Ma as best age estimate for RG-114 (Fig. 3c).

RG-114 cassiterite shows growth zoning in CL images. The U content of LA-ICP-MS data is relatively low with an average value of 3.5 ± 1.9 μg g^{-1}. The calculated f_{206} values are relatively low, ranging from 0.10% to 5.01% (Table 3). In the Tera-Wasserburg diagram, twenty-four LA-SF-ICP-MS analyses of cassiterite sample RG-144 yield an intercept age of 1015 ± 12 Ma (2 s, MSWD = 0.3; Fig. 4e), which is consistent with the ^{207}Pb-corrected $^{206}Pb/^{238}U$ age of 1014 ± 14 Ma. The ^{208}Pb based-common Pb corrected data constrain a concordia age of 1016 ± 12 Ma (2 s, MSWD = 2.9) and a corrected weighted mean $^{206}Pb/^{238}U$ age of 1017 ± 14 Ma (Fig. 4f). These results are consistent with our ID-TIMS ages and a published muscovite Ar—Ar age from the same area (1024.3 ± 5.5 Ma, Dewaele et al., 2015).

4.1.4. BB#7 (Maine)

U—Pb ID-TIMS dating of cassiterite sample BB#7 has been undertaken in two laboratories and two very different methods. Data obtained at GFZ are shown as red ellipses in Fig. 3f. The individual fractions have $^{206}Pb/^{204}Pb$ values in the range of 52.6 to 244.7 (Table 2). Total Pb and U contents of cassiterite sample BB#7 vary from 0.5 to 0.8 μg g^{-1} and from 6.2 to 9.6 μg g^{-1}, respectively. The corrected apparent $^{206}Pb/^{238}U$ ages range from 259.4 ± 2.2 Ma and 262.8 ± 2.3 Ma. All six aliquots fall on the concordia in the Wetherill diagram and yield a corrected concordia age of 261.6 ± 1.0 Ma (2 s, MSWD = 0.1) and a corrected weighted average $^{206}Pb/^{238}U$ age of 261.7 ± 1.5 Ma (2 s, MSWD = 1.4). Data obtained at Tianjin Institute of Geology and Mineral Resources are shown as green ellipses in Fig. 3f. Ten fractions were analysed. All analyses define a corrected concordia age of 263.4 ± 0.8 Ma (2 s, MSWD = 0.1) and a corrected weighted average $^{206}Pb/^{238}U$ age of 263.6 ± 1.6 Ma (2 s, MSWD = 0.2). The ID-TIMS results from two different laboratories agree with each other within uncertainties. The corrected weighted average $^{206}Pb/^{238}U$ age of all samples is 262.2 ± 0.8 Ma.

Cassiterite sample BB#7 is compositionally zoned (CL image Fig. 1e). It has low common Pb contents with f_{206} values ranging from 0.40% to 3.15% (Table 3). The U contents of this sample commonly show little variation with an average value of 22.8 ± 6.9 (2 s) μg g^{-1} (there is one LA-ICP-MS spot with a high U content of 53.0 μg g^{-1}, Table 1S). Twenty-three analyses yield an intercept age of 262.9 ± 3.2 Ma (2 s, MSWD = 0.3) in the Tera-Wasserburg diagram and a ^{207}Pb-corrected $^{206}Pb/^{238}U$ age of 262.8 ± 3.2 Ma (Fig. 5e). The ^{208}Pb based-common Pb corrected data yield a concordia age of 261.1 ± 3.2 Ma (2 s, MSWD = 1.5) and weighted average $^{206}Pb/^{238}U$ age of 261.0 ± 3.3 Ma (Fig. 5f). The age obtained by LA-SF-ICP-MS is identical with the average ID-TIMS age and is in good agreement with the ages of other pegmatites in the same area (Bradley et al., 2016).

4.1.5. AY-4 (Hunan province, China)

Six fractions of cassiterite sample AY-4 were analysed using ID-TIMS. The total Pb and U contents range from 0.7 to 6.4 μg g^{-1} and from 10.4 to 71.8 μg g^{-1}, respectively (Table 2). The measured $^{206}Pb/^{204}Pb$ varies from 42.1 to 81.7 μg g^{-1}. The corrected apparent $^{206}Pb/^{238}U$ ID-TIMS ages of the individual fractions vary from 153.9 ± 1.5 Ma to 154.6 ± 1.6 Ma (Table 3). In the Wetherill diagram, the six AY-4 aliquots overlap with each other and yield a corrected concordia age of 154.3 ± 0.8 Ma (2 s, MSWD = 0.1; Fig. 3d) and a corrected weighted average $^{206}Pb/^{238}U$ age of 154.3 ± 0.7 Ma (2 s, MSWD = 0.1). This age is younger than the $^{206}Pb/^{238}U$ ID-TIMS age of 158.2 ± 0.4 Ma reported by Yuan et al. (2011) and it is slightly older than the age of 151.9 ± 2.2 Ma reported by Carr et al. (2020). The possible causes for this age discrepancy are discussed later.

The LA-SF-ICP-MS data of cassiterite sample AY-4 have relatively high U contents of 15.2 to 320.0 μg g^{-1}. f_{206} shows a relatively large variation from 0.17% to 9.34% (Table 3). Thirty analyses yield an intercept age of 155.5 ± 1.1 Ma (2 s, MSWD = 0.1) in the Tera-Wasserburg diagram and define a ^{207}Pb-corrected $^{206}Pb/^{238}U$ age of 155.5 ± 1.1 Ma (Fig. 7a). For comparison, the ^{208}Pb-corrected data constrain a concordia age of 154.5 ± 1.1 Ma (2 s, MSWD = 1.0) and a

weighted average $^{206}Pb/^{238}U$ age of 154.5 ± 1.1 Ma (Fig. 7b).

4.1.6. 19GX (Guangxi province, China)

Five aliquots of cassiterite sample 19GX have been analysed by ID-TIMS. The measured $^{206}Pb/^{204}Pb$ ratios of sample 19GX fall in the range of 73.3 and 161.6. The contents of total Pb and U range from 0.2 to 0.3 μg g^{-1} and 7.6 to 13.0 μg g^{-1}, respectively (Table 2). The corrected apparent $^{206}Pb/^{238}U$ ages are very consistent and range from 99.7 ± 0.7 Ma to 100.1 ± 0.8 Ma. All measured aliquots overlap with each other within uncertainty and give a corrected concordia age of 100.0 ± 0.3 Ma (2 s, MSWD = 1.3; Fig. 3e). The five aliquots yield a corrected weighted average $^{206}Pb/^{238}U$ age of 100.0 ± 0.3 Ma (2 s, MSWD = 0.2).

The U contents of cassiterite sample 19GX obtained by LA-SF-ICP-MS are more variable than those obtained by ID-TIMS and range from 3.3 to 67.3 μg g^{-1} (Table 3). Most f_{206} values are below 3% except for one analysis with an exceptionally high common Pb contribution. All 21 analyses yield an intercept age of 100.3 ± 1.5 Ma (2 s, MSWD = 0.1) in the Tera-Wasserburg diagram and a ^{207}Pb-corrected $^{206}Pb/^{238}U$ age of 100.2 ± 1.5 Ma (Fig. 7c). The ^{208}Pb based-common Pb corrected data constrain a concordia age of 99.8 ± 1.5 Ma (2 s, MSWD = 1.0) and a $^{206}Pb/^{238}U$ age of 99.9 ± 1.5 Ma, respectively (Fig. 7d). The LA-SF-ICP-MS and ID-TIMS ages are identical and in good agreement with earlier reported zircon and cassiterite ages from the same deposit (Zhang et al., 2020).

4.2. Samples studied only by LA-SF-ICP-MS

4.2.1. Kard

Cassiterite sample Kard shows growth zoning (Fig. 1d). Its U contents range from 1.6 to 10.0 μg g^{-1} and its f_{206} values range from 0.20% to 7.73% (Table 3). Twenty-one analyses yield an intercept age of 429.1 ± 6.4 Ma (2 s, MSWD = 0.4) in the Tera-Wasserburg diagram and a ^{207}Pb-corrected $^{206}Pb/^{238}U$ age of 429.3 ± 6.4 Ma (Fig. 5a). The ^{208}Pb-corrected data yield a concordia age of 427.5 ± 6.4 Ma (2 s, MSWD = 2.5) and a weighted average $^{206}Pb/^{238}U$ age of 427.9 ± 6.7 Ma (Fig. 5b). Our cassiterite U—Pb age is older than the earlier reported ID-TIMS and LA-ICP-MS cassiterite ages (416 ± 1 Ma and 426 ± 13 Ma) for the same deposit (Deng et al., 2017). Our LA-SF-ICP-MS age, however, is consistent with earlier reported SHRIMP and LA-ICP-MS zircon ages (430–420 Ma, Bao et al., 2008; Li et al., 2012; Gao et al., 2014). W—Sn mineralization in the Kekekaerde deposit is associated with the 430 Ma monzogranite (Gao et al., 2014). A previous study indicates that the relative extended evolution of the system with several generations of hydrothermal fluids may cause the slight variation in mineralization age (Deng et al., 2017).

4.2.2. Zinnwald

Cassiterite sample Zinnwald shows considerable variations in U content (1.7 to 13.1 μg g^{-1}; Table 3). The f_{206} values show a relatively narrow range from 0.14% to 5.38%. All analysis spots cluster close to the discordia in the Tera-Wasserburg diagram and yield an intercept age of 321.9 ± 5.2 Ma (2 s, MSWD = 0.2) with a ^{207}Pb-corrected $^{206}Pb/^{238}U$ age of 321.8 ± 5.4 Ma (Fig. 5c). This agrees well with the ^{208}Pb-corrected concordia age of 319.6 ± 5.2 Ma (2 s, MSWD = 2.0) and the corrected weighted mean $^{206}Pb/^{238}U$ age of 321.5 ± 5.4 Ma (Fig. 5d). Our cassiterite U—Pb age agrees with the U—Pb cassiterite age of 321.5 ± 3.1 Ma reported by Zhang et al. (2017) from the same location and the U—Pb zircon and *Re*—Os molybdenite isochron ages of related rocks (324–318 Ma, Romer et al., 2007, 2010; Ackerman et al., 2017).

4.2.3. Yankee

Cassiterite sample Yankee is characterized by large variations in U content (1.3 to 125.3 μg g^{-1}) and f_{206} (0.06% to 23.9%). Most analyses have f_{206} less than 5%. Twenty-four analyses constrain an intercept age of 246.4 ± 2.9 Ma (2 s, MSWD = 0.4) in the Tera-Wasserburg diagram along with a ^{207}Pb-corrected $^{206}Pb/^{238}U$ age of 247.0 ± 2.6 Ma (Fig. 6a). However, published ID-TIMS data indicate that this sample has relatively radiogenic initial $^{207}Pb/^{206}Pb$ ratio (0.741 ± 0.007; Carr et al., 2020). In this study, this sample gives an $^{207}Pb/^{206}Pb$ intercept of 0.722 ± 0.075, i.e., a radiogenic initial $^{207}Pb/^{206}Pb$ ratio. This samples gives an intercept age of 244.6 ± 3.3 Ma (2 s, MSWD = 0.2, n = 24) and a corrected weighted mean $^{206}Pb/^{238}U$ age of 244.3 ± 2.6 Ma without anchoring the upper intercept. The unanchored intercept age is approximately 1% younger than the anchored intercept age for an initial $^{207}Pb/^{206}Pb$ ratio of 0.852 ± 0.017 as estimated from the S&K model (Stacey and Kramers, 1975). The anchored and unanchored ages agree within their uncertainties. Our results are in agreement with the ^{208}Pb-corrected concordia and weighted average $^{206}Pb/^{238}U$ ages of 246.2 ± 2.6 Ma and 246.3 ± 2.7 Ma, respectively (Fig. 6b). Our laser ablation data are consistent with previously reported ID-TIMS cassiterite age 246.48 ± 0.51 Ma (Carr et al., 2020).

4.2.4. Els

Cassiterite sample Els shows oscillatory zoning in CL images (Fig. 1h). The U contents and f_{206} values range from 0.9 to 35.1 μg g^{-1} and 0.14% to 4.36%, respectively (Table 3). In the Tera-Wasserburg diagram, all twenty-four analyses fall very close to the concordia and define an intercept age of 246.0 ± 4.4 Ma (2 s, MSWD = 0.3) and a ^{207}Pb-corrected $^{206}Pb/^{238}U$ age of 245.6 ± 4.3 Ma (Fig. 6c). For comparison, the ^{208}Pb-corrected data yield a concordia age of 244.0 ± 4.2 Ma (2 s, MSWD = 1.0) and a weighted average $^{206}Pb/^{238}U$ age of 244.2 ± 4.3 Ma (Fig. 6d). The cassiterite U—Pb age is slightly younger than the previously reported SHRIMP U—Pb zircon age of 250.3 ± 1.8 Ma (Cross and Blevin, 2013).

4.2.5. XBD-W

Sample XBD-W is characterized by the very low U contents (0.5 to 4.8 μg g^{-1}). The f_{206} values exhibit relatively large variations from 1.42% to 21.79% (Table 3). Seventeen analyses yield an intercept age of 198.0 ± 5.6 Ma (2 s, MSWD = 0.1) in the Tera-Wasserburg diagram and a ^{207}Pb-corrected $^{206}Pb/^{238}U$ age of 199.6 ± 4.1 Ma (Fig. 6e). The ^{208}Pb-corrected Pb data yield a concordia age of 195.9 ± 4.0 Ma (2 s, MSWD = 0.1) and a $^{206}Pb/^{238}U$ age of 195.9 ± 4.1 Ma, respectively (Fig. 6f). These ages agree well with previously reported ages form the same deposit (200–192 Ma, Cao et al., 2002; Liu et al., 2007a, 2007b, Liu et al., 2010; Zhang et al., 2014).

4.2.6. Y724

Cassiterite sample Y724 is rich in U with contents ranging from 92.4 to 449.2 μg g^{-1}. The common Pb contribution in cassiterite sample Y724 is highly variable, ranging from 0.24% to 13.77% (Table 3). Twenty-four analyses yield an intercept age of 78.3 ± 0.9 Ma (2 s, MSWD = 0.5) in the Tera-Wasserburg diagram and a ^{207}Pb-corrected $^{206}Pb/^{238}U$ age of 78.3 ± 0.9 Ma (Fig. 7e). These ages are consistent with the concordia age of 77.7 ± 0.9 Ma and the weighted average $^{206}Pb/^{238}U$ age of 77.7 ± 0.9 Ma obtained for the ^{208}Pb-corrected data (Fig. 7f). Our results are in good agreement with previously reported zircon and cassiterite U—Pb ages (79.2–78.5 Ma, Hu et al., 2020) and molybdenite *Re*—Os ages (78.8–77.0 Ma, Zheng et al., 2016; Hu et al., 2020) for the same deposit.

4.3. Element mapping of cassiterite

The trace element mapping of cassiterite sample Kard is shown in Fig. 8. Other cassiterite samples show similar element distribution patterns. Sample Kard is characterized by relatively high contents of high field strength elements (HFSE: Ti, Zr, Nb, Hf, Ta) ranging from several hundreds to several thousands μg g^{-1} (Fig. 8). In particular Ti, Nb, and Ta show pronounced oscillatory zoning. The contents of these elements are highly correlated. Oscillatory zoning is also observed for Zr and Hf. The zoning of these two elements is not as pronounced as the zoning for Ti, Nb, and Ta and the highest contents of Zr and Hf do not occur in those parts of the crystal that have the highest contents of Ti, Nb, and Ta.

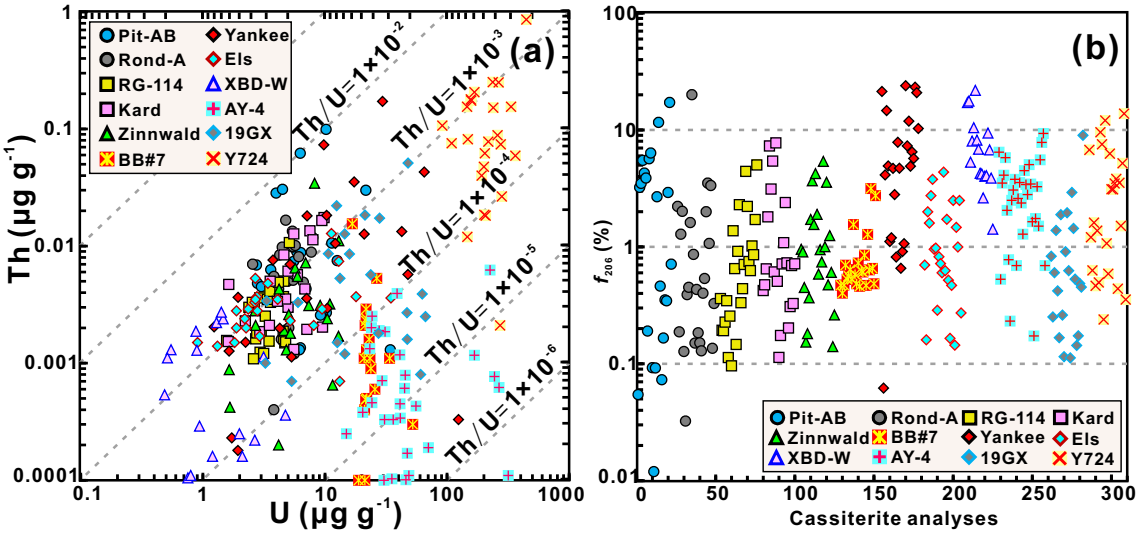

Fig. 2. (a) Comparison between U and Th concentrations in cassiterite. (b) The f_{206} value represents the percentage of common ^{206}Pb in total ^{206}Pb of the analysed cassiterite samples.

In some sections of the cassiterite sample Kard, the contents of Ca and W are particularly high. The high W contents are not related to substitutions of W in the cassiterite lattice, but to the presence of scheelite and wolframite along fractures and old crystal surfaces within the analysed cassiterite sample (Fig. 8). Such an intergrowth of cassiterite with scheelite and wolframite has been described before for the Kekekaerde W—Sn deposit (Deng et al., 2017). The highest contents of U and Pb, both reaching contents up to c. 30 μg g^{-1}, are obtained in the zones with the highest contents of Ca and W, indicating that scheelite is the major carrier of U and common Pb. There are sections with very low Pb contents and moderate U contents that are particularly suitable for U—Pb dating by LA-ICP-MS.

Tin is six-fold coordinated in cassiterite. For six-fold coordination, Sn^{4+} has an ionic radius of 0.69 Å (Shannon, 1976). Elements that substitute for tin to variable extent include Ti^{4+} (0.61 Å), Zr^{4+} (0.72 Å), Nb^{5+} (0.64 Å), Hf^{4+} (0.71 Å), Ta^{5+} (0.64 Å), and W^{6+} (0.74 Å), in part in combination with Fe^{3+} (0.55 Å) and Sc^{3+} (0.75 Å) for charge balance (Möller and Dulski, 1983; Möller et al., 1988; Plimer et al., 1991; Murciego et al., 1997; Cheng et al., 2019). Among the HFSE, Zr^{4+} has a slightly larger ionic radius and, therefore, does not correlate well with the other HFSE. Similarly, substitution of W is irregular, in part as W-minerals, such as scheelite and wolframite, may grow together with cassiterite and in part as W^{6+}, which has a similar ionic radius as Sn^{4+}, has a major charge difference.

The Pb and U contents in cassiterite are low compared to Zr, largely as these elements are too large to fit into six-fold coordinated cation sites and for Pb also because of the charge difference. For instance, Pb^{2+} has an ionic radius of 1.19 Å and U^{4+} has an ionic radius of 0.89 Å (Shannon, 1976). Both elements mainly occur in defects, inclusions, and zones of major substitution of other elements. In cassiterite sample Kard, higher U contents in cassiterite are mainly found in domains with higher contents of HFSE. This relation, however, seems not to be generally applicable as Cheng et al. (2019) did not observe a general correlation between the contents of U and the HFSE. The variation of U content in cassiterite samples is probably related to the availability of U and, thus, the U content of the fluid. The element maps show no clear relation between the contents of Pb and other elements in cassiterite.

5. Discussion

5.1. Isobaric interferences

The signal for ^{202}Hg is commonly used to correct the interference of ^{204}Hg on the ^{204}Pb signal during LA-ICPMS analysis of zircon. This correction, however, cannot be used for W-bearing minerals, such as wolframite, ixiolite and cassiterite, because of interferences of $^{186}W^{18}O$ on ^{204}Hg and ^{204}Pb as well as $^{186}W^{16}O$ and $^{184}W^{18}O$ on ^{202}Hg (Yang et al., 2020; Carr et al., 2017; Neymark et al., 2018). As shown in Fig. 9b, the 202 mass signal (^{202}Hg and $^{184}W^{18}O$) is slightly higher after the end of ablation than before the start of ablation of the cassiterite sample. Such a difference for background signals of 202 mass before and after analysis is not observed for NIST SRM 612 glass (Fig. 9a), which implies that the memory effect is related to the analysed cassiterite sample (Fig. 9b). Therefore, tungsten oxides show a memory effect after the laser has been turned off (Fig. 9b). Such a memory effect also was reported for wolframite U—Pb dating by laser ablation (Yang et al., 2020).

The ^{204}Pb correction procedure is the ideal procedure for the common Pb contribution as ^{204}Pb is the only non-radiogenic Pb isotope. The ^{204}Pb correction in LA-ICP-MS dating, however, is compromised by low signal intensity and isobaric interference (^{204}Hg and $^{186}W^{18}O$ on ^{204}Pb). Therefore, the ^{204}Pb correction procedure for the common Pb contribution is not feasible in this case. Instead, the common Pb contribution has to be corrected using the ^{207}Pb or ^{208}Pb correction procedures, respectively. The basic idea is the following: The measured ^{206}Pb, ^{207}Pb, and ^{208}Pb consist of a contribution of common Pb and radiogenic Pb and the ratios $^{207}Pb/^{206}Pb$ and $^{208}Pb/^{206}Pb$ vary over time. The isotopic composition of common Pb can be estimated reasonably well in most cases by using the composition of typical crustal lead of the appropriate age (e.g., Stacey and Kramers, 1975) or can be obtained from the measurement of Pb-rich cogenetic phases (free of notable contents of U and Th) such a feldspar or sulphide minerals. The correction procedure using S&K model Pb, however, is problematic for anomalously radiogenic initial Pb. For instance, Yankee cassiterite has a relatively radiogenic initial $^{207}Pb/^{206}Pb$ ratio. Using the S&K model Pb will produce a too old intercept age. The ^{208}Pb correction is given in formula I and II

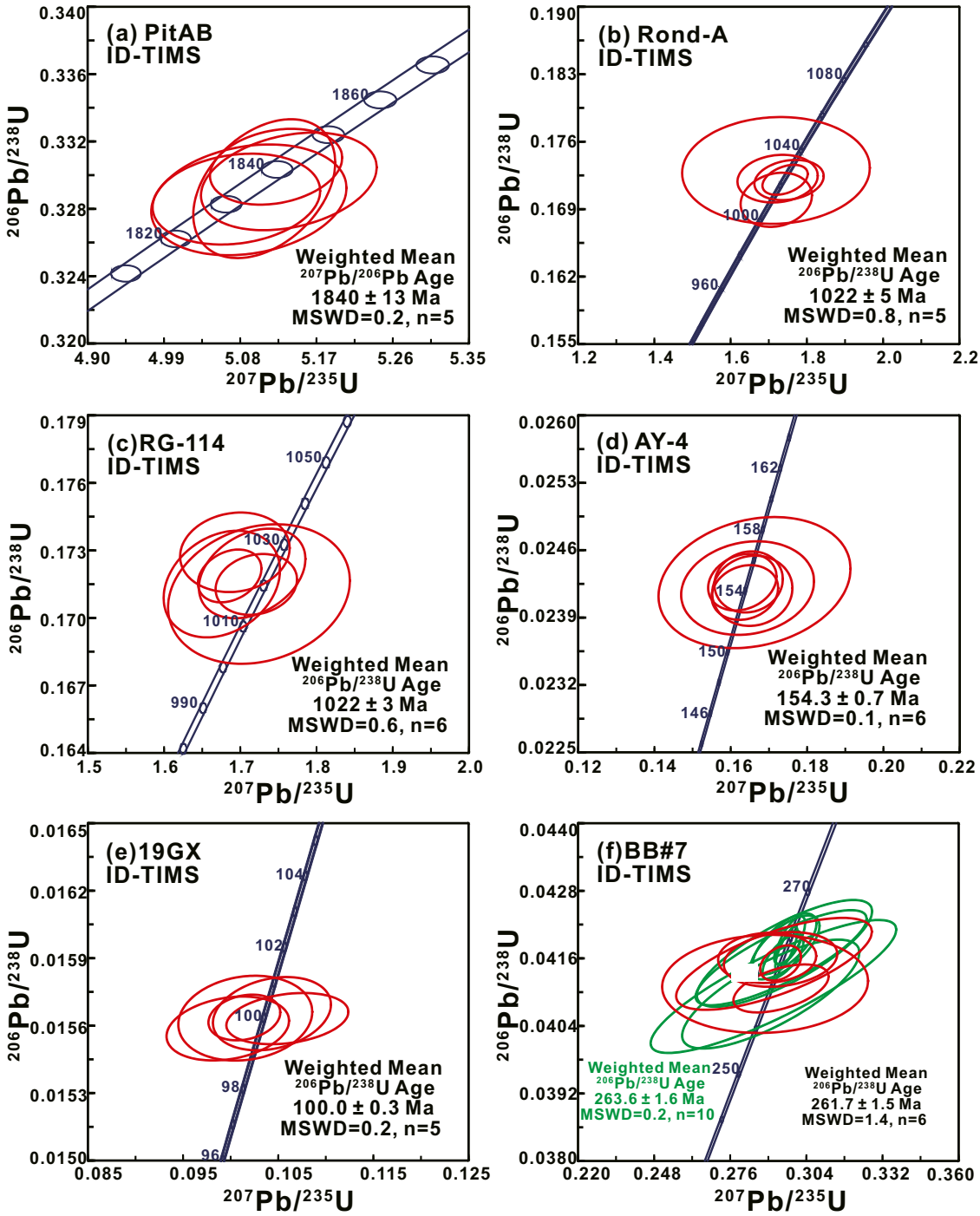

Fig. 3. Concordia diagrams for ID-TIMS U—Pb results. Sample BB#7 has been analysed in two different laboratories.

(method section), the ^{207}Pb correction works in an analogue way. Commonly, the ^{207}Pb/^{206}Pb correction is preferred over the ^{208}Pb correction as the ^{207}Pb/^{206}Pb of Proterozoic and Phanerozoic common Pb varies in a relatively narrow range (^{207}Pb/^{206}Pb = 1.05 to 0.87). Any of these corrections works reasonably well for samples that are not dominated by common Pb contributions. For cassiterite the ^{208}Pb-correction is commonly preferable because cassiterite typically contains very little Th (Th/U $\langle 10^{-2}$), which implies that the measured ^{208}Pb essentially corresponds to the originally incorporated common Pb (Zack et al., 2011; Neymark et al., 2018).

5.2. *Feasibility of ^{208}Pb correction procedure*

The feasibility of the ^{208}Pb correction procedure in U—Pb cassiterite dating is illustrated in two ways, i.e., by calculating the maximum effect of in situ ^{208}Pb growth on the obtained ages and by comparing the ages obtained using the ^{208}Pb and the ^{207}Pb correction procedures for the same analytical data. We use Fig. 10 to illustrate the effect of radiogenic growth of ^{208}Pb on the ^{208}Pb correction procedure, using (i) the equation for the ^{208}Pb correction (Eq. 1, above), (ii) the appropriate common ^{208}Pb/^{206}Pb ratio (using typical crustal Pb, e.g., Stacey and Kramers,

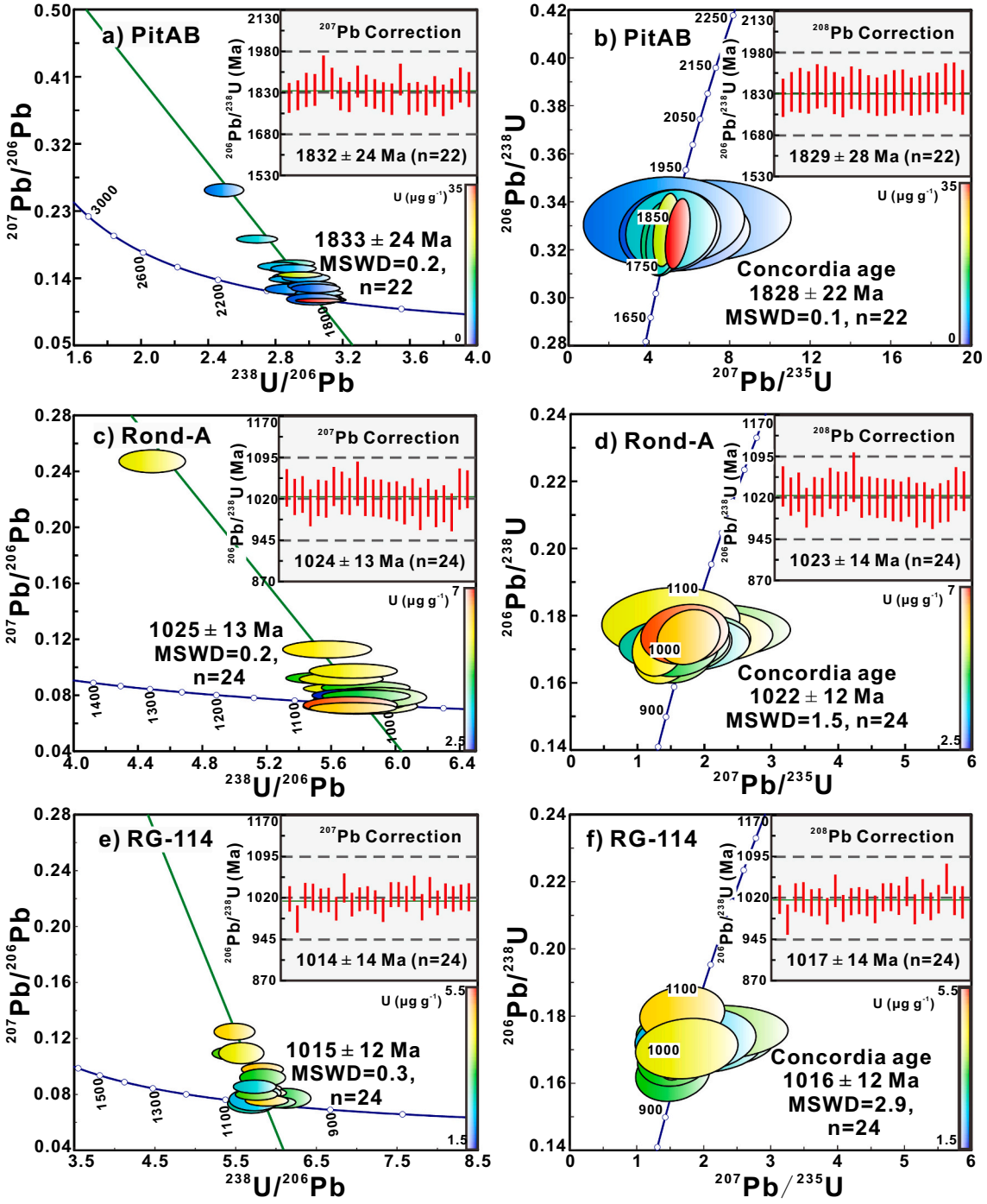

Fig. 4. LA-SF-ICP-MS U—Pb data of cassiterite samples PitAB, Rond-A, and RG-114. The Tera-Wasserburg diagram and the ^{207}Pb corrected weighted average $^{206}Pb/^{238}U$ ages (inset) are shown in the left column, the ^{208}Pb corrected concordia diagram and the weighted average $^{206}Pb/^{238}U$ ages are shown in the right column.

1975) and (iii) Th/U ratios ranging from 0.001 to 0.1. As the $^{208}Pb/^{206}Pb$ ratio of average crust varies with time, the horizontal axis also represents a non-linear time scale. The vertical axis represents the proportion of common Pb if the effect of in situ ^{208}Pb growth had been neglected. The black solid lines show the systematic error due to unaccounted radiogenic ^{208}Pb for different Th/U ratios and ages. The systematic error becomes more important for samples with a higher Th/U or an older age (Fig. 10). All studied cassiterite samples have extremely low Th concentrations and low Th/U ratios (Fig. 2a). For the highest measured Th/U ratio of 0.01, i.e., the worst-case scenario, the radiogenic growth of ^{208}Pb contributes less than 0.15% to the initial ^{208}Pb for an age of 3000 Ma. Such a small miscalculation of the common Pb contribution has barely any effect on the final ages, especially in comparison with the commonly obtained analytical precision of 2–3% for cassiterite laser ablation data. For higher Th/U ratios, the effect on the U—Pb age becomes larger. For instance, for a Th/U ratio of 0.1, the ^{208}Pb correction will result in apparent $^{206}Pb/^{238}U$ cassiterite ages that are up to 1.50% too young for Phanerozoic cassiterite. For all cassiterite samples reported in this study, the Th/U ratios are below 0.01. Therefore, the ^{208}Pb correction procedure can be applied to all cassiterite samples.

We compare intercept ages obtained for measured data in the Tera-

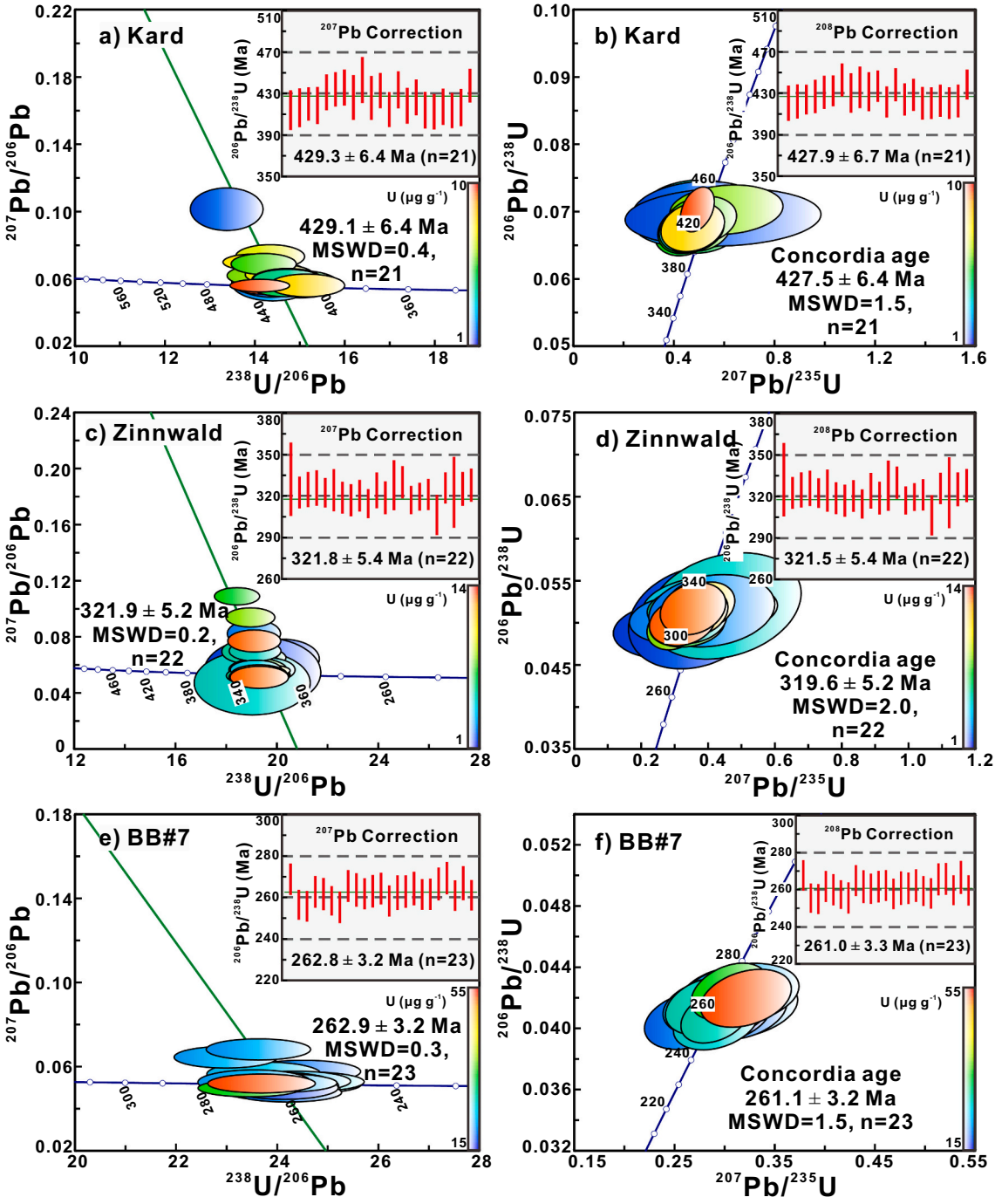

Fig. 5. LA-SF-ICP-MS U—Pb data of cassiterite samples Kard, Zinnwald, and BB#7. The Tera-Wasserburg diagram and the ^{207}Pb corrected weighted average ^{206}Pb/^{238}U ages (inset) are shown in the left column, the ^{208}Pb corrected concordia diagram and the weighted average ^{206}Pb/^{238}U ages are shown in the right column.

Wasserburg diagram with weighted average ^{206}Pb/^{238}U ages obtained for data corrected for common Pb using the ^{207}Pb correction and the ^{208}Pb correction, respectively (Figs. 4, 5, 6, and 7). The various analyses fall on and above the reverse concordia in the Tera-Wasserburg diagram and define intercept ages that are in good agreement with the corresponding ^{207}Pb corrected and ^{208}Pb corrected weighted average ^{206}Pb/^{238}U ages. The ^{208}Pb corrected results show a slightly systematic offset to younger ages than ^{207}Pb corrected results, which probably could be accounted for matrix difference between cassiterite and NIST 614 glass. In general, the ^{207}Pb corrected and the ^{208}Pb corrected weighted average ^{206}Pb/^{238}U ages are identical within uncertainties, which shows that the measured ^{208}Pb allows for a reliable correction of the common Pb contribution in cassiterite.

The trace elements mapping could provide important information for understanding the petrogenesis as well as guiding in situ U—Pb analysis. A range of non-destructive imaging techniques were used for the sample screening, including optical microscopy, CL image, and back-scattered imaging (BSE). These techniques were commonly used to identify the internal features of the cassiterite, but not for the identification of high U and low Pb contents domains. Alternatively, LA-ICP-MS mapping techniques not only provide an opportunity to investigate more detailed information across complexly heterogeneous samples, but also could be

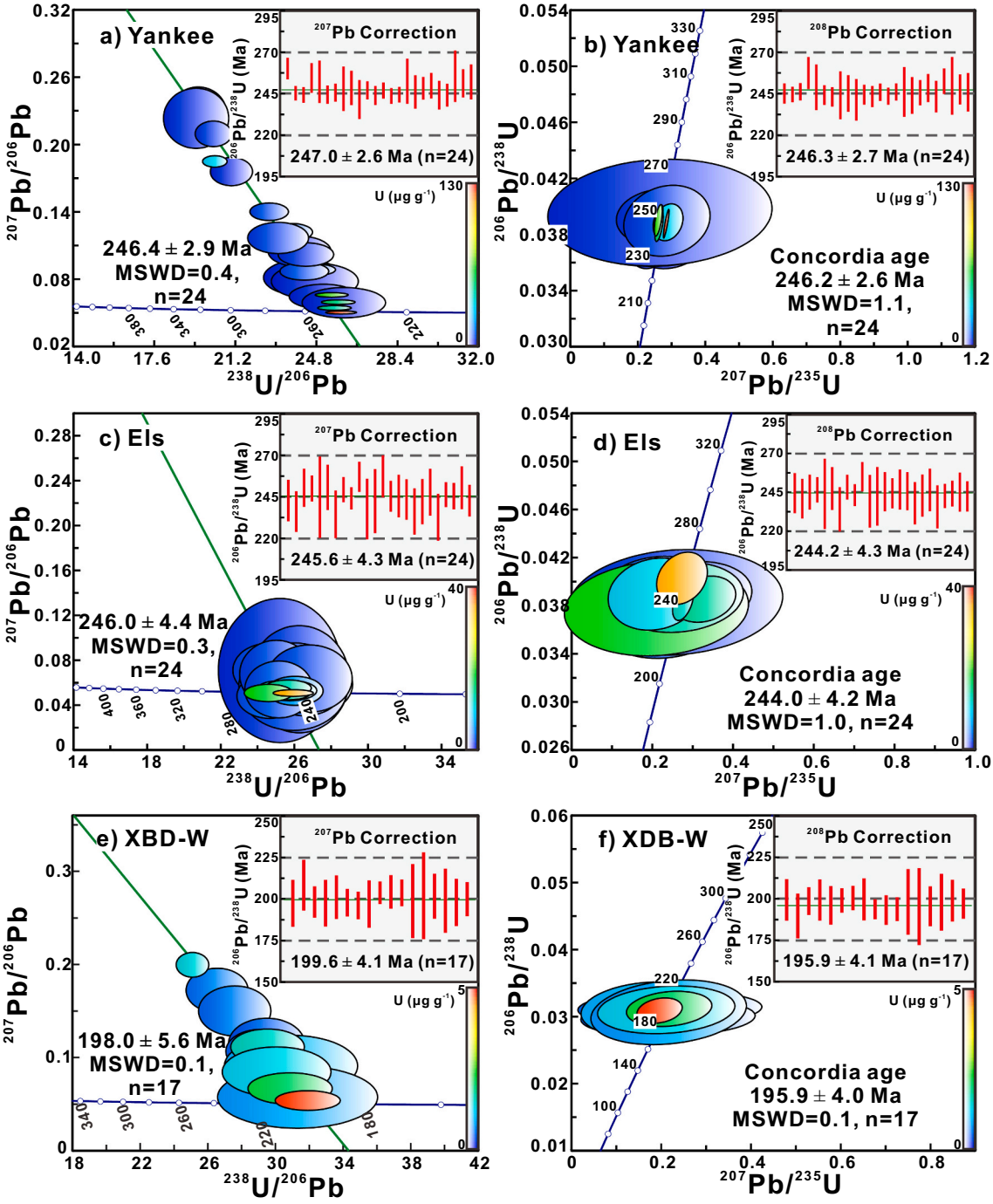

Fig. 6. LA-SF-ICP-MS U—Pb data of cassiterite samples Yankee, Els, and XBD-W. The Tera-Wasserburg diagram and the ^{207}Pb corrected weighted average $^{206}Pb/^{238}U$ ages (inset) are shown in the left column, the ^{208}Pb corrected concordia diagram and the weighted average $^{206}Pb/^{238}U$ ages are shown in the right column.

used to determine both the location and nature of U and Pb zonings in the unknown samples. Image-guided LA-ICP-MS U—Pb cassiterite dating allows to identifying domains that have the same origin and age for analysis using distribution maps of characteristic major and trace elements (Chew et al., 2021).

5.3. Age discrepancy of the AY-4 cassiterite

In this study, the initial $^{206}Pb/^{204}Pb$ and $^{207}Pb/^{204}Pb$ ratios of AY-4 cassiterite were calculated using the $^{206}Pb/^{204}Pb$ vs. $^{238}U/^{204}Pb$ diagram and the $^{207}Pb/^{204}Pb$ vs. $^{206}Pb/^{204}Pb$ diagram ($^{206}Pb/^{204}Pb = 18.9 \pm 0.5$, $^{207}Pb/^{204}Pb = 15.7 \pm 0.15$, and $^{208}Pb/^{204}Pb = 38.0 \pm 1.0$). The estimated initial Pb isotopic composition is slightly less radiogenic than the one used by Carr et al. (2020; $^{206}Pb/^{204}Pb = 19.9 \pm 1.6$ and $^{207}Pb/^{204}Pb = 15.75 \pm 0.15$) that was also determined from isochron relationships. The measured Pb isotopic compositions is not very radiogenic. The analysed fractions of cassiterite sample AY-4 have $^{206}Pb/^{204}Pb$ ratios that range from 42.1 to 81.7 (Table 2). For such low $^{206}Pb/^{204}Pb$ ratios, the composition of the Pb isotopic composition employed for the common Pb correction has a major effect on the apparent $^{206}Pb/^{238}U$ ages. Estimating the isotopic composition of common Pb using isochron diagrams results in internally consistent concordant data in the $^{207}Pb/^{235}U$ vs. $^{206}Pb/^{238}U$ diagram, but does not necessarily imply that the chosen value is correct. A different common

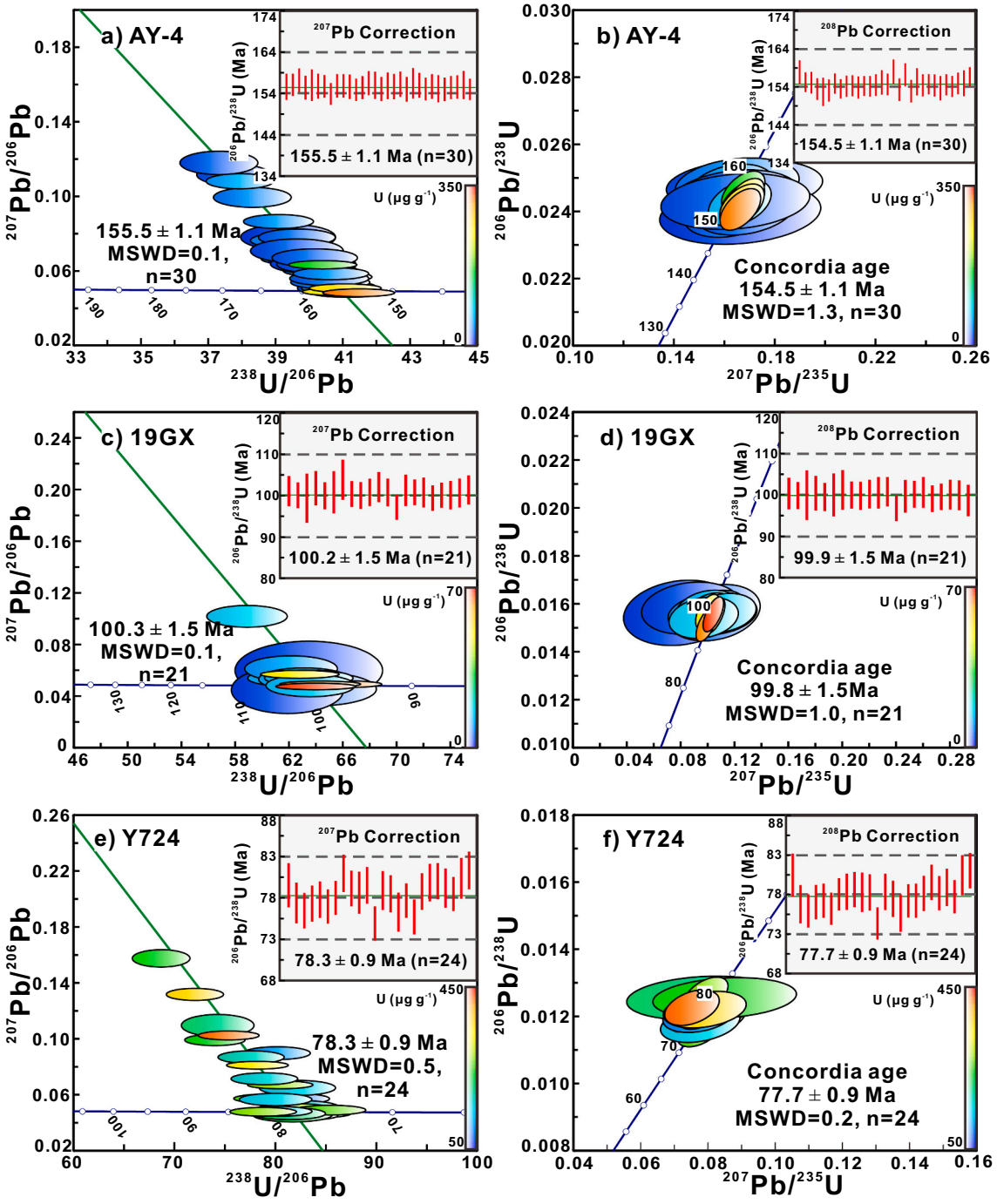

Fig. 7. LA-SF-ICP-MS U—Pb data of cassiterite samples AY-4, 19GX, and Y724. The Tera-Wasserburg diagram and the ^{207}Pb corrected weighted average ^{206}Pb/^{238}U ages (inset) are shown in the left column, the ^{208}Pb corrected concordia diagram and the weighted average ^{206}Pb/^{238}U ages are shown in the right column.

Pb isotopic composition would result in different apparent ^{206}Pb/^{238}U ages and – because of the large uncertainty of the ^{207}Pb/^{235}U age – still yield seemingly concordant data. We use Fig. 11 to illustrate the effect of the common Pb correction on the apparent ^{206}Pb/^{238}U age and to test whether the here used common Pb isotopic composition is geologically reasonable.

Cassiterite analysis C5–2 (Table 2) with a ^{206}Pb/^{204}Pb ratio of 79.1 was used to illustrate the dependence of the U—Pb age on the isotopic composition of the used common Pb. Figure 11 shows the variation of the ^{206}Pb*/^{238}U and ^{207}Pb*/^{235}U ages as a function of the common Pb composition (see also Romer, 1992). The ^{206}Pb*/^{238}U ages are shown by the vertical solid lines, whereas the difference between the ^{206}Pb*/^{238}U and ^{207}Pb*/^{235}U ages is shown by the oblique grey lines. The 0 Ma isoline corresponds to the common Pb compositions that produce concordant cassiterite ages. Isolines with a negative offset represent normal discordant ages, whereas isolines with a positive offset correspond to reversely discordant ages. The lower the measured ^{206}Pb/^{204}Pb, the more sensitive is the obtained ^{206}Pb*/^{238}U age on the common Pb correction. Note, the difference between the AY-4 age presented here and the age presented by Carr et al. (2020) may be caused by the different initial Pb isotopic composition used for data reduction and does not have to imply sample heterogeneity.

Li et al. (2007) reported the lead isotope data from the Furong tin deposit and the spatially and temporally associated A-type Qitianling

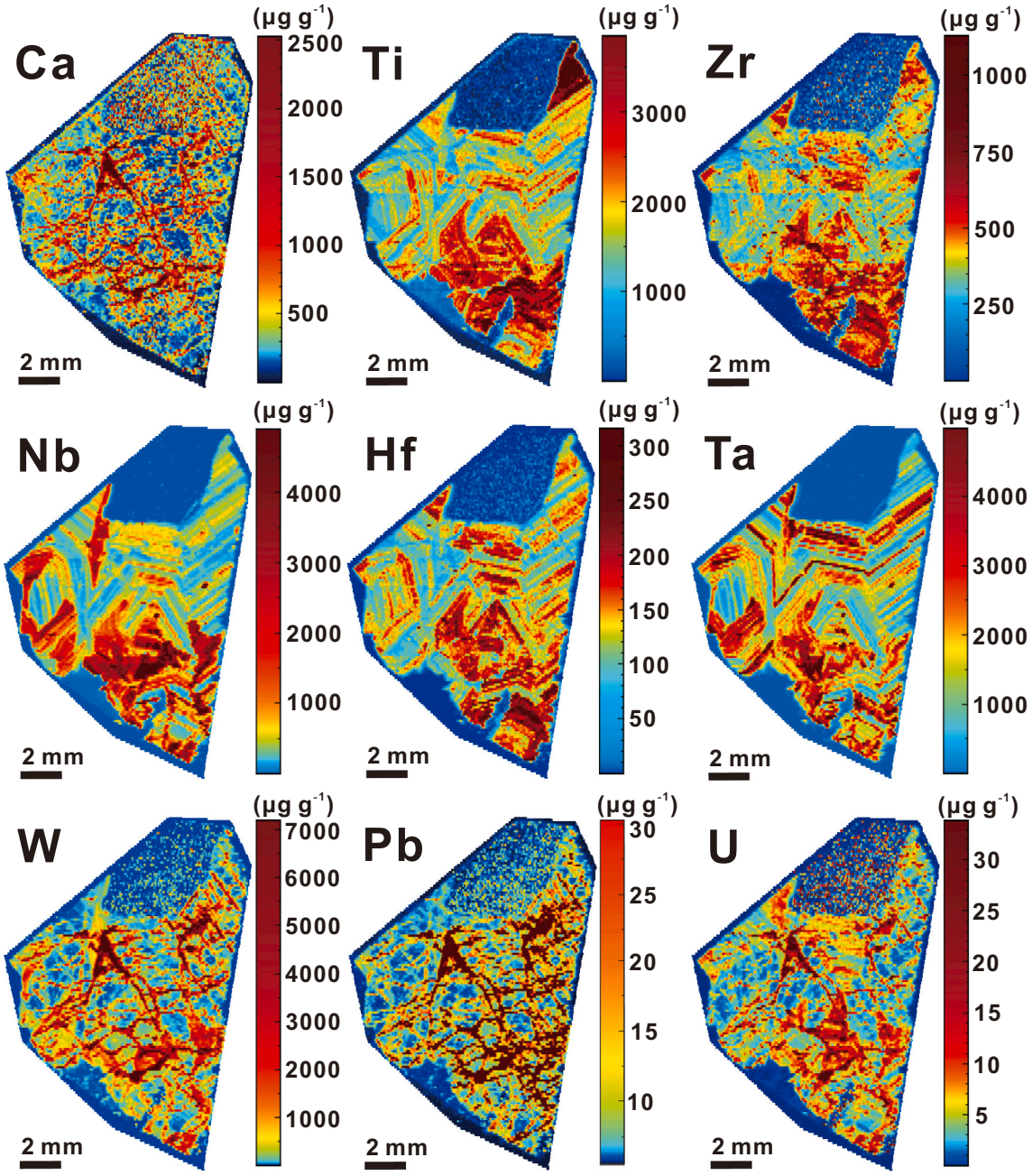

Fig. 8. Element mapping of representative cassiterite sample Kard.

granite. Lead isotope data from feldspar from the granite (yellow diamonds) and sulfide minerals (green triangles) are broadly overlapping and fall in the $^{206}Pb/^{204}Pb$ and $^{207}Pb/^{204}Pb$ ranges of 18.4 to 18.8 and 15.50 to 15.77, respectively (Fig. 11.). For comparison, the $^{206}Pb/^{204}Pb$ and $^{207}Pb/^{204}Pb$ ratios used for the common Pb correction were 18.9 ± 0.5 and 15.70 ± 0.15, respectively. Thus, the used initial Pb isotopic composition is geologically reasonable and, therefore, the obtained age ID-TIMS U—Pb age of 154.3 ± 0.7 Ma for AY-4 cassiterite seems to be preferable over ages obtained using a different initial Pb isotopic composition.

Most cassiterite samples investigated by ID-TIMS (Pit-AB, RG-114, BB#7 and 19GX) in this study have isochron intercepts are consistent with the S&K values within uncertainty. Sample Rond-A is an exception. The isochron intercepts of this sample give a radiogenic initial $^{207}Pb/^{206}Pb$ ratio of 0.774 ± 0.261. Using the S&K value at 1.0 Ga (0.910 ± 0.018, Stacey and Kramers, 1975) for the common Pb correction of the ID-TIMS data would give an age older than 1.08 Ga, which is not geologically reasonable. The LA-SF-ICP-MS data of cassiterite samples Rond-A cluster close to the concordia, implying that the sample has a relatively low common Pb content and the choice of the initial Pb isotopic composition does not affect the intercept age of this sample significantly.

5.4. Suitability for use as in situ U—Pb cassiterite reference materials

The U—Pb analytical data of the cassiterite samples investigated by LA-SF-ICP-MS are summarized in Table 3. Among these samples, AY-4 cassiterite is the most commonly used reference material for U—Pb dating by laser ablation (Yuan et al., 2011). The study of Carr et al. (2020) presented a younger age for AY-4 cassiterite, which could imply that this cassiterite is not homogeneous or the original age is too old. Our ID-TIMS data have low measured $^{206}Pb/^{204}Pb$ ratios and the age is

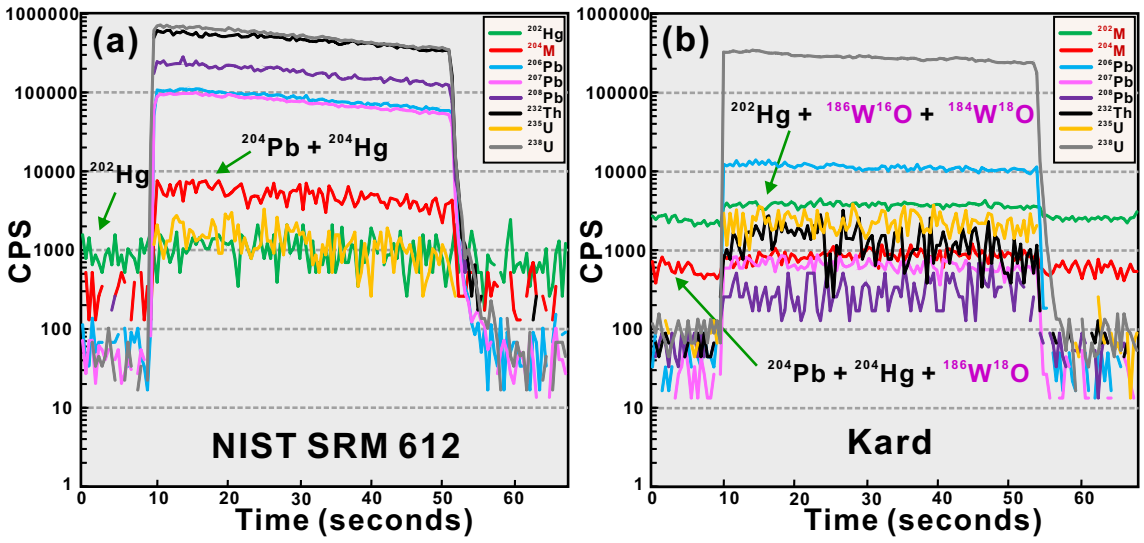

Fig. 9. Time vs. signal sensitivity for a typical LA-SF-ICP-MS analysis of (a) reference material NIST SRM612 and (b) cassiterite sample Kard. The ^{202}M signal is evidently elevated in sample Kard (b) when laser was turned off compared with that in NIST SRM 612.

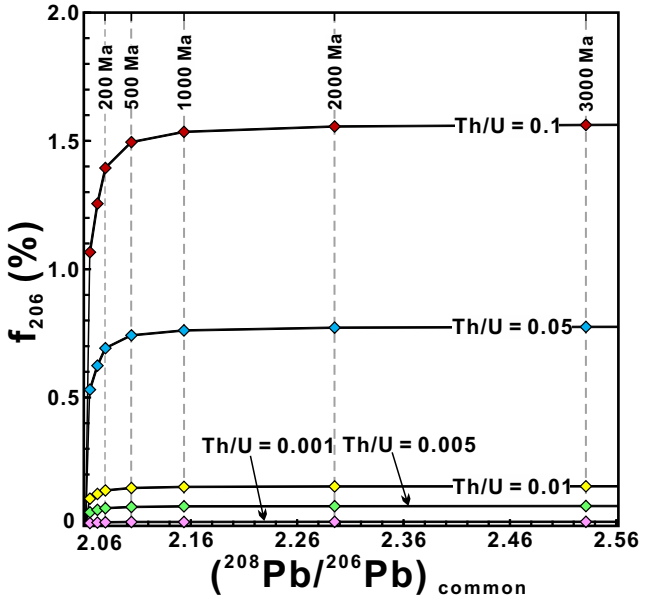

Fig. 10. The ^{208}Pb correction of common Pb introduces a small systematic error if it is assumed that all ^{208}Pb present in cassiterite is common Pb. The size of this error depends on the Th/U and the age of the sample. The higher Th/U and the older the sample, the larger becomes the error. The f_{206} (%) shows the size of overestimation of the common Pb correction (leading to too young ^{206}Pb/^{238}U ages) depending on the age of the sample (here shown as the ^{208}Pb/^{206}Pb ratio of common Pb based on the two-stage crustal model of Stacey and Kramers, 1975). For Th/U less than 0.01, the resulting error of the ^{208}Pb correction on the common Pb contribution is less than 0.15%. As cassiterite has Th/U values that typically are less than 0.01, the 208Pb correction yields correct ages within uncertainties. Diagram calculated using 9.8485 E^{-10} y^{-1} and 1.55125 E^{-10} y^{-1} for the decay constants for ^{235}U and ^{238}U, respectively.

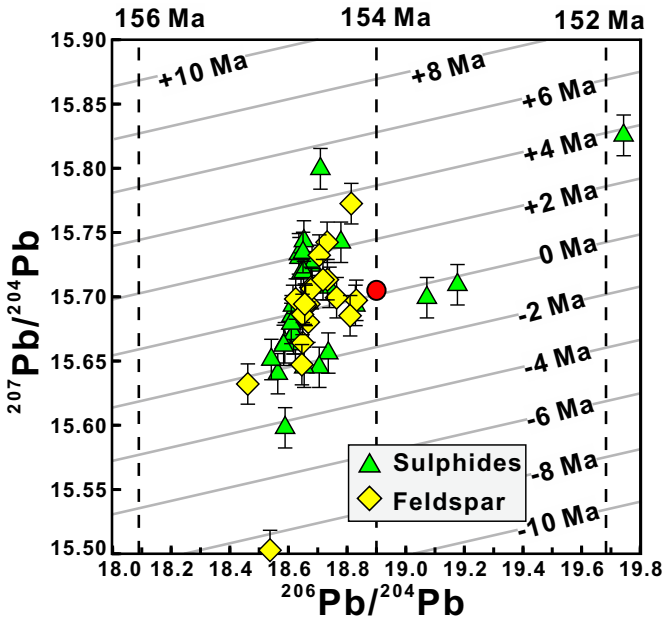

Fig. 11. Diagram illustrating the relation between the isotopic composition of the common Pb correction and the age of low-^{238}U/^{204}Pb phases, such as cassiterite. The dashed vertical lines correspond to the ^{206}Pb/^{238}U ages for the corresponding ^{206}Pb/^{204}Pb of the common Pb. The grey solid lines show the difference between the ^{206}Pb/^{238}U and ^{207}Pb/^{235}U ages. The "0 Ma" line corresponds to the concordia, negative offsets correspond to normally discordant data. The grid is calculated for sample C5–2 (AY-4 cassiterite) from Table 2 (^{206}Pb/^{204}Pb = 79.1). The initial Pb isotopic composition used for calculation of the ^{206}Pb/^{204}Pb ages is shown as red dot. For samples with a higher measured ^{206}Pb/^{204}Pb, the lines of identical age are more widely spaced. Lead isotopic compositions of sulphides from the Furong tin deposit (green triangles) and feldspar from associated granite (yellow diamonds) are from Li et al. (2007). Uncertainties the common Pb isotopic composition is given with 0.1% error bars. The Pb isotopic data from Li et al. (2007) were given an error about. The ages were calculated using ^{238}U/^{235}U = 137.88 and the decay constants for ^{235}U and ^{238}U of 9.8485 *E*-10 y^{-1} and 1.55125 E-10 y^{-1}, respectively. (For interpretation of the references to colour in this figure legend, the reader is referred to the web version of this article.)

sensitive to the initial Pb isotopic composition used for data reduction. Our data indicate that the age of AY-4 cassiterite is close the 154.3 ± 0.7 Ma (2 s). Considering the present uncertainty concerning the age homogeneity of cassiterite AY-4, this sample should not be used as a primary reference material. PitAB and Rond-A were investigated by Neymark et al. (2018), PitAB and Rond-A show very good reproducibility and the ID-TIMS and LA-SF-ICP-MS U—Pb ages agree well with

previously reported results (Neymark et al., 2018). PitAB and Rond-A contain variable and relatively high common Pb contents (f_{206} ranging from 0.01% to 17.17% and from 0.03% to 19.97%, respectively), which could still be used as reference material following the method of Chew et al. (2014). Cassiterite samples RG-114, BB#7, and 19GX are reported for the first time in this study. Each of them shows very limited variation in the common Pb content. Their ID-TIMS ages are consistent with the ages obtained by LA-SF-ICP-MS. Therefore, these three materials can be used as primary reference materials for cassiterite U—Pb dating.

We determined the U—Pb cassiterite ages of samples Kard, Zinnwald, Yankee, Els, XBD-W, and Y724 only by LA-SF-ICP-MS. Among these samples, Yankee, XBD-W, and Y724 show a relatively large variation in common Pb composition. The LA-SF-ICP-MS U—Pb ages of these samples agree well with known ID-TIMS and LA-ICP-MS results from the same locations. Despite the variable common Pb content, Yankee still can serve as a primary reference material due to consistent ages obtained using different methods. Cassiterite sample XDB-W has relatively low U contents, making it more difficult to get a precise age. Therefore, XDB-W represents a reliable secondary reference material, but should not be used as a primary reference material. Cassiterite sample Y724 has the highest U contents among the samples analysed here. Due to its relatively high U content, it could be used as primary reference material once it has been dated by ID-TIMS method. Samples Kard, Zinnwald, and Els contain relatively low common Pb contents. All analyses of these samples cluster very close to the concordia in the Tera-Wasserburg diagram. Therefore, they can serve as good reference material candidates once their ages have been confirmed by ID-TIMS U—Pb dating.

6. Conclusions

We presented an analytical protocol for in situ U—Pb dating of cassiterite by LA-SF-ICP-MS. Cassiterite investigated in this study originates from different tin deposits and pegmatites with ages ranging from ~78 Ma to ~1840 Ma. The obtained in situ cassiterite U—Pb ages are consistent within uncertainty with our ID-TIMS ages on aliquots from the same samples or ages for the same deposit from the literature. Our results demonstrate the applicability of the used analytical protocol for cassiterite samples of a broad range of ages.

There is significant interference of tungsten oxides on ^{202}Hg, ^{204}Hg, and ^{204}Pb, which implies that common Pb has to be corrected using the ^{207}Pb or ^{208}Pb correction. Cassiterite is characterized by extremely low Th/U ratios (Th/U < 0.01) and the measured ^{208}Pb is predominantly non-radiogenic, which implies that ^{208}Pb can be used to correct common Pb contributions. The ^{208}Pb-corrected data yield ages that are in good agreement with non-corrected intercept ages in the Tera-Wasserburg diagram and ages calculated from ^{207}Pb corrected data. Because of the limited ingrowth of radiogenic ^{208}Pb in cassiterite, the ^{208}Pb correction procedure is preferable for cassiterite.

We characterized several cassiterite samples that potentially could be used as reference materials for LA-ICP-MS U—Pb dating of cassiterite. We recommend cassiterite samples RG-114, BB#7, and 19GX as primary reference materials for in situ cassiterite U—Pb dating. Samples PitAB, Rond-A and Yankee, which have relatively high common Pb contents could also be used as primary reference materials after common Pb correction. Cassiterite samples Kard, Zinnwald, and Els are also suited as primary reference materials, but their U—Pb ages have to be confirmed by ID-TIMS. Cassiterite samples XBD-W, and Y724 show a large range of common Pb contents and have not been dated by ID-TIMS, therefore, they can only serve as secondary reference material. Our new ID-TIMS U—Pb age of cassiterite reference material AY-4 of 154.3 ± 0.7 Ma differs from previously reported ID-TIMS ages, largely due the initial common Pb composition and not the age heterogeneity of the sample.

Declaration of Competing Interest

The authors declare that they have no known competing financial interests or personal relationships that could have appeared to influence the work reported in this paper.

Acknowledgements

This work was financially supported by National Natural Science Foundation of China (Grants 41525012, 41688103 & 42103025). The work of Ming Yang at GFZ was supported by the China Scholarship Council (202004910582). We are indebted to Leonid A. Neymark (SPG-IV, Pit AB, and Rond-A), Ting-Guang Lan (Kard), Hui-Qing Huang (Yankee and Elsmore), Qian Ma (XBD-W), Shun-Da Yuan (AY-4), Xiao-Feng Li (19GX), Hong Zhong (Y724), and Tony Nikischer (BB#7 and Zinnwald) for providing cassiterite samples. We thank Patrick Carr and David Chew for careful reviews and Balz Kamber for efficient edditorial handling of the manuscript. Small aliquots of samples RG-114, BB#7, and 19GX may be obtained from Yue-Heng Yang.

Appendix A. Supplementary data

Supplementary data to this article can be found online at https://doi.org/10.1016/j.chemgeo.2022.120754.

References

Ackerman, L., Haluzová, E., Creaser, R.A., Pašava, J., Veselovský, F., Breiter, K., Erban, V., Drábek, M., 2017. Temporal evolution of mineralization events in the Bohemian Massif inferred from the Re-Os geochronology of molybdenite. Mineral. Deposita 52, 651–662.

Bao, Y.F., Liu, Y.J., Wang, X.C., 2008. Relations between Bashierxi granite, west Dong Kunlun and Baiganhu tungsten-tin deposit. Jilin Geol. 27, 56–59 (in Chinese with English abstract).

Bettencourt, J.S., Tosdal, R.M., Leite Jr., W.B., Payolla, B.L., 1999. Mesoproterozoic rapakivi granites of Rondônia tin province, southwestern border of the Amazonian craton, Brazil: I. Reconnaissance U–Pb geochronology and regional implications. Precambrian Res. 95, 41–67.

Bradley, D., Shea, E., Buchwaldt, R., Bowring, S., Benowitz, J., O'Sullivan, P., McCauley, A., 2016. Geochronology and tectonic context of lithium-cesium-tantalum pegmatites in the Appalachians. Can. Mineral. 54, 945–969.

Caley, E.R., 1932. The action of hydroiodic acid on stannic oxide. J. Am. Chem. Soc. 54, 3240–3243.

Cao, Z.M., Zheng, J.B., Li, Y.G., Ren, J.G., Xu, S.J., Wang, R.C., Shoji, T., Kaneda, H., Kabayashi, S., 2002. Geologic and geochemical features of the volatile-rich ore fluid and its tracing and dating in the Xuebaoting beryl-scheelite vein deposit China. Sci. China D-Earth Sci. 32, 719–729.

Carr, P.A., Norman, M.D., Bennett, V.C., 2017. Assessment of crystallographic orientation effects on secondary ion mass spectrometry (SIMS) analysis of cassiterite. Chem. Geol. 467, 122–133.

Carr, P.A., Zink, S., Bennett, V.C., Norman, M.D., Amelin, Y., 2020. A new method for U-Pb geochronology of cassiterite by ID-TIMS applied to the Mole Granite polymetallic system, eastern Australia. Chem. Geol. 539, 119539.

Chen, J., Hou, K.J., Wang, Q., Yuan, S.D., Chen, Y.L., 2021. In situ U-Pb dating of cassiterite by LA-ICP-MS without a matrix-matched standard. Acta Petrol. Sin. 37, 943–955.

Cheng, Y.B., Spandler, C., Kemp, A., Mao, J.W., Rusk, B., Hu, Y., Blake, K., 2019. Controls o cassiterite (SnO_2) crystallization: evidence from cathodoluminescence, trace-element chemistry, and geochronology at the Gejiu Tin District. Am. Mineral. 104, 118–129.

Chew, D.M., Petrus, J.A., Kamber, B.S., 2014. U/Pb LA–ICPMS dating using accessory mineral standards with variable common Pb. Chem. Geol. 363, 185–199.

Chew, D.M., Drost, K., Marsh, J.H., Petrus, J.A., 2021. LA-ICP-MS imaging in the geosciences and its applications to geochronology. Chem. Geol. 559, 119917.

Cross, A.J., Blevin, P.L., 2013. Summary of results for the joint GSNSW-GA geochronology project: New England Orogen 2009–2010. Geoscience Australia, Record 2013/27. In: Geological Survey of New South Wales, Report GS2013/0426.

Deng, X.H., Chen, Y.J., Bagas, L., Zhou, H.Y., Zheng, Z., Yue, S.W., Chen, H.J., Li, H.M., Tu, J.R., Cui, Y.R., 2017. Cassiterite U-Pb geochronology of the Kekekaerde W-Sn deposit in the Baiganhu ore field, East Kunlun Orogen, NW China: timing and tectonic setting of mineralization. Ore Geol. Rev. 100, 534–544.

Dewaele, S., Muchez, Ph., Bugress, R., Boyce, A., 2015. Geological setting and timing of the cassiterite vein type mineralization of the Kalima area (Maniema, Democratic Republic of Congo). J. Afr. Earth Sci. 112, 199–212.

Gao, Y.B., Li, W.Y., Li, Z.M., Wang, J., Hattori, K.K., Zhang, Z.W., Geng, J.Z., 2014. Geology, geochemistry, and genesis of tungsten-tin deposits in the Baiganhu district, Northern Kunlun belt, Northwestern China. Econ. Geol. 109, 1787–1799.

Gemmrich, L., Torró, L., Melgarejo, J.C., Laurent, O., Vallance, J., Chelle-Michou, C., 2021. Trace element composition and U-Pb ages of cassiterite from the Bolivian tin belt. Mineral. Deposita. https://doi.org/10.1007/s00126-020-01030-3.

Griffin, W.L., Powell, W.J., Pearson, N.J., O'Reilly, S.Y., 2008. GLITTER: data reduction software for laser ablation ICP-MS. In: Sylvester, P. (Ed.), Laser Ablation-ICP-MS in

the Earth Sciences: Current Practices and Outstanding Issues. Min. Ass. Can. Short Course, 40, pp. 308–311.
Gulson, B.L., Jones, M.T., 1992. Cassiterite: potential for direct dating of mineral deposits and a precise age for the Bushveld complex granites. Geology 20, 355–358.
Hu, P.C., Zhu, W.G., Zhong, H., Zhang, R.Q., Zhao, X.Y., Mao, W., 2020. Late Cretaceous granitic magmatism and Sn mineralization in the giant Yinyan porphyry tin deposit, South China: constraints from zircon and cassiterite U–Pb and molybdenite Re–Os geochronology. Mineral. Deposita 56, 743–765.
Jaffey, A.H., Flynn, K.F., Glendenin, L.E., Bentley, W.C., Essling, A.M., 1971. Precision measurement of half-lives and specific activities of ^{235}U and ^{238}U. Phy. Rev. C 4, 1889–1906.
Jiang, S.Y., Zhao, K.D., Jiang, H., Su, H.M., Xiong, S.F., Xiong, Y.Q., Xu, Y.M., Zhang, W., Zhu, L.Y., 2020. Spatiotemporal distribution, geological characteristics and metallogenic mechanism of tungsten and tin deposits in China: an overview (in Chinese with English abstract). Chin. Sci. Bull. 65, 86–101.
Jochum, K.P., Weis, U., Stoll, B., Kuzmin, D., Yang, Q.C., Raczek, I., Jacob, D.E., Stracke, A., Birbaum, K., Frick, D.A., Günther, D., Enzweiler, J., 2011. Determination of Reference Values for NIST SRM 610-617 Glasses Following ISO Guidelines Geostand. Geoanal. Res. 35, 397–429.
Kleeman, J.D., Plimer, I.R., Lu, J., Foster, D.A., Davidson, R., 1997. Timing of thermal and mineralisation events associated with the Mole Granite. In: Ashley, P., Flood, P. G. (Eds.), Tectonics and Metallogenesis of the New England Orogen. Geol. Soc. Australia, Spec. Publ, 19, pp. 254–265.
Lehmann, B., 1982. Metallogeny of tin: magmatic differentiation versus geochemical heritage. Econ. Geol. 77, 50–59.
Li, Z.L., Hu, R.Z., Yang, J.S., Peng, J.T., Li, X.M., Bi, X.W., 2007. He, Pb and S isotopic constraints on the relationship between the A-type Qitianling granite and Furong tin deposit, Hunan Province, China. Lithos 97, 161–173.
Li, G.C., Feng, C.Y., Wang, R.J., Ma, S.C., Li, H.M., Zhou, A.S., 2012. SIMS Zircon U-Pb Age, petrochemistry and tectonic implications of granitoids in Northeastern Baiganhu W-Sn orefield, Xinjiang. Acta Geosci. Sin. 33, 216–226 (in Chinese with English abstract).
Liu, Y., Deng, J., Li, C.F., Shi, G.H., Zheng, A.L., 2007a. REE composition in scheelite and scheelite Sm–Nd dating for Xuebaoding W–Sn–Be deposit. Sichuan. Chin. Sci. Bull. 52, 2543–2550.
Liu, Y.P., Li, Z.X., Li, H.M., Guo, L.G., Xu, W., Ye, L., Li, C.Y., Pi, D.H., 2007b. U–Pb geochronology of cassiterite and zircon from the Dulong Sn–Zn deposit: evidence for Cretaceous large-scale granitic magmatism and mineralization events in south eastern Yunnan province, China. Acta Petrol. Sin. 23, 967–976 (in Chinese with English abstract).
Liu, Y., Deng, J., Zhang, G.B., Shi, G.H., Yang, L.Q., Wang, Q.F., 2010. ^{40}Ar/^{39}Ar dating of Xuebaoding granite in the Songpan–Garzê orogenic belt, southwest China, and its geological significance. Acta Geol. Sin. 84, 345–357 (English Edition).
Ludwig, K.R., 2003. ISOPLOT 3.0-a geochronological toolkit for Microsoft Excel. In: Berkeley Geochronology Center Special Publication, No. 4.70.
Luo, T., Hu, Z.C., Zhang, W., Liu, Y.S., Zong, K.Q., Zhou, L., Zhang, J.F., Hu, S.H., 2018. Water vapor-assisted "universal" nonmatrix-matched analytical method for the in Situ U–Pb dating of zircon, monazite, titanite, and xenotime by laser ablation-inductively coupled plasma mass spectrometry. Anal. Chem. 90, 9016–9024.
Möller, P., Dulski, P., 1983. Fractionation of Zr and Hf in cassiterite. Chem. Geol. 40, 1–12.
Möller, P., Dulski, P., Szacki, W., Malow, G., Riedel, E., 1988. Substitution of tin in cassiterite by tantalum, niobium, tungsten, iron and manganese. Geochim. Cosmochim. Acta 52, 1497–1503.
Murciego, A., Sanchez, A.G., Dusausoy, Y., Pozas, J.M.M., Ruck, R., 1997. Geochemistry and EPR of cassiterites from the Iberian Hercynian Massif. Min. Mag. 61, 357–365.
Neto, A.C.B., Ferron, J.T.M.M., Chauvet, A., Chemale Jr., F., de Lima, E.F., Barbanson, L., Costa, C.F.M., 2014. U–Pb dating of the Madeira Suite and structural control of the albite-enriched granite at Pitinga (Amazonia, Brazil): evolution of the A-type magmatism and implications for the genesis of the Madeira Sn–Ta–Nb (REE, cryolite) world-class deposit. Precambrian Res. 243, 181–196.
Neymark, L.A., Holm-Denoma, C.S., Moscati, R.J., 2018. In situ LA-ICPMS U–Pb dating of cassiterite without a known-age matrix-matched reference material: Examples from worldwide tin deposits spanning the Proterozoic to the Tertiary. Chem. Geol. 483, 410–425.
Neymark, L.A., Holm-Denoma, C.S., Larin, A.M., Moscati, R.J., Plotkina, Y.V., 2021. LA-ICPMS U-Pb dating reveals cassiterite inheritance in the Yazov granite, Eastern Siberia: Implications for tin mineralization. Mineral. Deposita 56, 1177–1194.
Paton, C., Hellstrom, J., Paul, B., Woodhead, J., Hergt, J., 2011. Iolite: Freeware for the visualisation and processing of mass spectrometric data. J. Anal. At. Spectrom. 26, 2508–2518.
Paul, B., Paton, C., Norris, A., Woodhead, J., Hellstrom, J., Hergt, J., Greig, A., 2012. CellSpace: A module for creating spatially registered laser ablation images within the Iolite freeware environment. J.Anal. At. Spectrom. 27, 700–706.
Petrus, J.A., Chew, D.M., Leybourne, M.I., Kamber, B.S., 2017. A new approach to laser-ablation inductively-coupled-plasma mass-spectrometry (LA-ICP-MS) using the flexible map interrogation tool 'Monocle' Chem. Geol. 463, 76–93.
Plimer, I.R., Lu, J., Kleeman, J.D., 1991. Trace and rare earth elements in cassiterite—sources of components for the tin deposits of the Mole Granite, Australia. Mineral. Deposita 26, 267–274.
Rizvanova, N.G., Kuznetsov, A.B., 2020. A new approach to ID-TIMS U–Pb dating of cassiterite by the example of the pitkranta tin deposit. Dokl. Earth Sci. 491, 47–51.
Rizvanova, N.G., Skublov, S.G., Cheremazova, E.V., 2017. Age of hydrothermal processes in Central Iberian Zone (Spain) according to U-Pb dating of cassiterite and apatite. Zapiski Gornogo Instituta 225, 275–283.
Romer, R.L., 1992. Vesuvianite–new tool for the U-Pb dating of skarn ore deposits. Mineral. Petrol. 46, 331–341.
Romer, R.L., Lüders, V., 2006. Direct dating of hydrothermal W mineralization: U-Pb age for hübnerite ($MnWO_4$), Sweet Home Mine, Colorado. Geochim. Cosmochim. Acta 70, 4725–4733.
Romer, R.L., Thomas, R., Stein, H.J., Rhede, D., 2007. Dating multiply overprinted Sn-mineralized granites—an example from the Erzgebirge, Germany: Mineral. Deposita 42, 337–359.
Romer, R.L., Förster, H.J., Štemprok, M., 2010. Age constraints for the late-Variscan magmatism in the Altenberg-Teplice caldera (eastern Erzgebirge, Krušné hory): N. Jb. Mineral. Abh. 187, 289–305.
Schaltegger, U., Pettke, T., Audétat, A., Reusser, E., Heinrich, C.A., 2005. Magmatic-to-hydrothermal crystallization in the W–Sn mineralized Mole Granite (NSW, Australia): part I: crystallization of zircon and REE-phosphates over three million years—a geochemical and U–Pb geochronological study. Chem. Geol. 220, 215–235.
Schmid, R., Romer, R.L., Franz, L., Oberhänsli, R., Martinotti, G., 2003. Basement-Cover Sequences within the UHP unit of the Dabie Shan. J. Metamorph. Geol. 21, 531–538.
Shannon, R.D., 1976. Revised effective ionic radii and systematic studies of interatomic distances in halides and chalcogenides. Acta Cryst. A. 32, 751–767.
Stacey, J.S., Kramers, J.D., 1975. Approximation of terrestrial lead isotope evolution by a two-stage model. Earth Planet. Sci. Lett. 26, 207–221.
Swart, P.K., Moore, F., 1982. The occurrence of uranium in association with cassiterite, wolframite, and sulfide mineralization in South-West England. Mineral. Mag. 46, 211–215.
Tapster, S., Bright, J., 2020. High-precision ID-TIMS cassiterite U–Pb systematics using a low-contamination hydrothermal decomposition: implications for LA-ICP-MS and ore deposit geochronology. Geochron. 2, 425–441.
Tomascak, P.B., Krogstad, E.J., Walker, R.J., 1996. U-Pb monazite geochronology of granitic rocks from Maine: implications for late Paleozoic tectonics in the Northern Appalachians. J. Geol. 104, 185–195.
Wang, F., Bagas, L., Jiang, S., Liu, Y., 2017. Geological, geochemical, and geochronological characteristics of Weilasituo Sn-polymetal deposit, Inner Mongolia, China. Ore Geol. Rev. 80, 1206–1229.
Wu, S.T., Wörner, G., Jochum, K.P., Stoll, B., Simon, K., Kronz, A., 2019. The preparation and preliminary characterisation of three synthetic andesite reference glass materials (ARM-1, ARM-2, ARM-3) for in situ microanalysis geostand. Geoanal. Res. 43, 567–584.
Wu, S.T., Yang, M., Yang, Y.H., Xie, L.W., Huang, C., Wang, H., Yang, J.H., 2020. Improved in situ zircon U–Pb dating at high spatial resolution (5–16 μm) by laser ablation–single collector–sector field–ICP–MS using Jet sample and X skimmer cones. Int. J. Mass Spectrom. 456, 116394.
Yamazaki, E., Nakai, S., Yokoyama, T., Ishihara, S., Tang, H., 2013. Tin isotope analysis of cassiterites from Southeastern and Eastern Asia. Geochem. J. 47, 21–35.
Yang, M., Yang, Y.H., Wu, S.T., Romer, R.F., Che, X.D., Zhao, Z.F., Li, W.S., Yang, J.H., Wu, F.Y., Xie, L.W., Huang, C., Zhang, D., Zhang, Y., 2020. Accurate and precise in situ U-Pb dating of wolframite series minerals via LA-SF-ICP-MS. J. Anal. At. Spectrom. 35, 2191–2203.
Yang, Y.H., Yang, M., Wang, H., Yang, J.H., Wu, F.Y., 2021. Methodology for in situ wolframite U-Pb dating and its application. Sci. China Earth Sci. 64, 187–190.
Yuan, S.D., Peng, J.T., Hu, R.Z., Li, H.M., Shen, N.P., Zhang, D.L., 2008. A precise U–Pb age on cassiterite from the Xianghualing tin–polymetallic deposit (Hunan, South China). Mineral. Deposita 43, 375–382.
Yuan, S.D., Peng, J.T., Hao, S., Li, H.M., Geng, J.Z., Zhang, D.L., 2011. In situ LA-MC-ICPMS and ID-TIMS U–Pb geochronology of cassiterite in the giant Furong tin deposit, Hunan Province, South China: New constraints on the timing of tin–polymetallic mineralization. Ore Geol. Rev. 43, 235–242.
Zack, T., Stockli, D.F., Luvizotto, G.L., Barth, M.G., Belousova, E., Wolfe, M.R., Hinton, R. W., 2011. In situ U–Pb rutile dating by LA-ICP-MS: 208Pb correction and prospects for geological applications. Contrib. Mineral. Petrol. 162, 515–530.
Zagruzina, I.A., Pinskii, E.M., Savinova, I.V., 1987. Uranium in cassiterite of tin deposits. Int. Geol. Rev. 29, 94–109.
Zhang, D.L., Peng, J.T., Hu, R.Z., Yuan, S.D., Zheng, D.S., 2011. The closure of U-Pb isotope system in cassiterite and its reliability for dating. Geol. Rev. 57, 549–554 (in Chinese with English abstract).
Zhang, D.L., Peng, J.T., Coulson, I.M., Hou, L.H., Li, S.J., 2014. Cassiterite U–Pb and muscovite ^{40}Ar–^{39}Ar age constraints on the timing of mineralization in the Xuebaoding Sn–W–Be deposit, western China. Ore Geol. Rev. 62, 315–322.
Zhang, R.Q., Lehmann, B., Seltmann, R., Sun, W.D., Li, C.Y., 2017. Cassiterite U-Pb geochronology constrains magmatic-hydrothermal evolution in complex evolved granite systems: the classic Erzgebirge tin province (Saxony and Bohemia). Geology 45, 1095–1098.
Zhang, D., Zhao, K.D., Wang, B.D., Cheng, K.Y., Luo, X.L., Zhang, W., Li, Q., Jiang, S.Y., 2020. Cretaceous granitic magmatism and mineralization in the Shanhu W-Sn ore deposit in the Nanling Range in South China. Ore Geol. Rev. 126, 103758.
Zheng, W., Mao, J.W., Zhao, C.S., Ouyang, H.G., Wang, X.Y., 2016. Re–Os geochronology of molybdenite from Yinyan porphyry Sn deposit in South China. Resour. Geol. 66, 63–70.